Quaternary Research (2022), **106**, 28–43
doi:10.1017/qua.2021.56

Research Article

The signal of climate changes over the last two millennia in the Gulf of St. Lawrence, eastern Canada

Xiner Wu[a]*, Anne de Vernal[a], Bianca Fréchette[a], Matthias Moros[b] and Kerstin Perner[b]

[a]Geotop, Université du Québec à Montréal (UQAM), 201 avenue du Président Kennedy, Montréal, Québec H3C 3P8, Canada and [b]Leibniz Institute for Baltic Sea Research Warnemünde, Seestrasse 15, 18119, Rostock, Germany

Abstract

Climate changes over the past two millennia in the central part of the Gulf of St. Lawrence are documented in this paper with the aim of determining and understanding the natural climate variability and the impact of anthropogenic forcing at a regional scale. The palynological content (dinocysts, pollen, and spores) of the composite marine sediment core MSM46-03 collected in the Laurentian Channel was used to reconstruct oceanographic and climatic changes with a multidecadal temporal resolution. Sea-surface conditions, including summer salinity and temperature, sea-ice cover, and primary productivity, were reconstructed from dinocyst assemblages. Results revealed a remarkable cooling trend of about 4°C after 1230 cal yr BP (720 CE) and a culmination with a cold pulse dated to 170–40 cal yr BP (1780–1910 CE), which likely corresponds to the regional signal of the Little Ice Age. This cold interval was followed by a rapid warming of about 3°C. In the pollen assemblages, the decrease of *Pinus* abundance over the past 1700 yr suggests changes in wind regimes, likely resulting from increased southerly incursions of cold and dry Arctic air masses into southeastern Canada.

Keywords: Gulf of St. Lawrence, Sea-surface temperature, Sea-surface salinity, Sea-ice cover, Dinocysts, Pollen, Late Holocene, Palynology, Paleoclimate

(Received 5 February 2021; accepted 15 August 2021)

INTRODUCTION

The last 2000 yr represent an interval of interest for the study of natural climate variability and its interaction with anthropic activities. Climate changes during this interval are relatively well documented from European historical and climate proxy records as a succession of warm and cold phases associated with the Roman Warm Period, Dark Ages Cold Period, Medieval Warm Period, and Little Ice Age (LIA) (e.g., Desprat et al., 2003; Helama et al., 2017). However, little is known about the magnitude and pacing of climate changes in eastern Canada during this time interval because of limited historical data, the oldest dating from the European colonization in the sixteenth century (e.g., Ramsden, 1978).

In southeastern Canada, the Gulf of St. Lawrence (GSL) is an epicontinental sea connected to the North Atlantic through the Strait of Belle Isle and the Cabot Strait (Fig. 1). It is characterized by large amounts of freshwater runoff from the Great Lakes and the watershed of the St. Lawrence River (Koutitonsky and Bugden, 1991; Galbraith et al., 2019). Hence, the GSL behaves like a large estuarine system with strongly stratified waters. The shallow surface-water layer has high nutrient content, low thermal inertia, and very large seasonal temperature contrasts (Koutitonsky and Bugden, 1991; Saucier et al., 2003). The confluence of different air masses in the study region (Fig. 1) makes this an ideal location for reconstructing climate change associated with air-mass circulation patterns, while close linkages between the hydrological budget of the watershed and surface-water salinity provide complementary information for the interpretation of regional climate on land. It is also an area of high biological productivity and diversity, which plays a role in the carbon cycle. Understanding the response of this complex ecosystem to past climate changes is pivotal for predicting the impacts of future climate changes.

Instrumental observations reveal significant changes in the GSL region over the last decades. Warming and decreasing oxygen concentrations in the bottom waters causing hypoxia in the gulf and the lower St. Lawrence Estuary (SLE) have been recorded since the 1930s (Gilbert et al., 2005; Galbraith et al., 2019). Moreover, data indicate a marked decrease of sea ice since 2010 (Galbraith et al., 2019) and a general trend of increasing air temperature and sea-surface temperature (SST) of 0.9 ± 0.3°C and 0.5 ± 0.3°C per decade, respectively (Galbraith et al., 2012).

On longer timescales, beyond the recent instrumental records, some regional studies permit documentation of past climates from the analyses of micropaleontological and geochemical records of marine sediment cores as well as terrestrial and coastal sedimentary sequences. At the scale of the Holocene, the studies by de Vernal et al. (1993, 2013a), Levac (2001, 2003), Solignac et al. (2011), Dhahri (2010), Thibodeau et al. (2013), Balestra et al. (2013), and Lemay-Tougas (2014) led to reconstruction of sea-surface and bottom-water conditions at several sites from the

***Corresponding author at:** Geotop, Université du Québec à Montréal (UQAM), 201 avenue du Président Kennedy, Montréal, Québec H3C 3P8, Canada. E-mail address: xiner.wu02@gmail.com (X. Wu).

Cite this article: Wu X, de Vernal A, Fréchette B, Moros M, Perner K (2022). The signal of climate changes over the last two millennia in the Gulf of St. Lawrence, eastern Canada. *Quaternary Research* **106**, 28–43. https://doi.org/10.1017/qua.2021.56

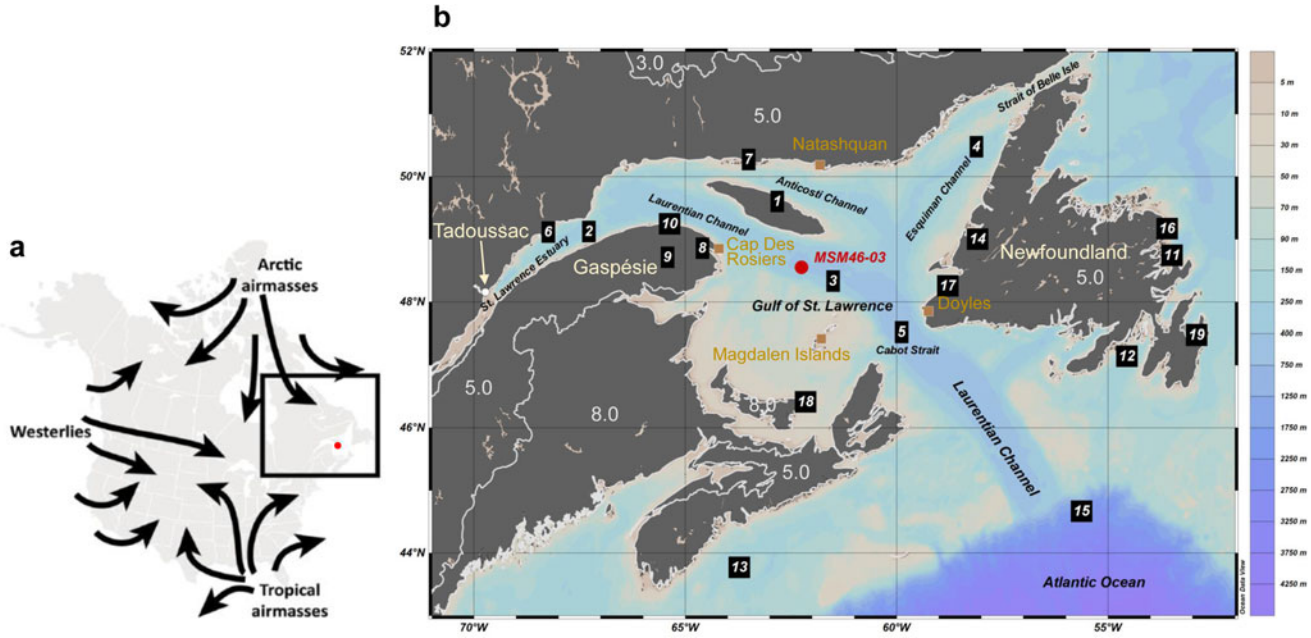

Figure 1. (a) Map of North America showing the main air-mass trajectories over eastern Canada (modified from Pratte et al., 2017). (b) Location map of core site MSM46-03 (in red), nearby climate stations (in yellow; Natashquan, Cap Des Rosiers, Doyles, Magdalen Islands), and level I ecoregions (white numbers) in areas surrounding the GSL as classified by the Commission for Environmental Cooperation (1997). Classification codes: 3.0, Taiga; 5.0, Northern Forests; 8.0, Eastern Temperate Forests. The numbers in black squares indicate the location of cores and study sites mentioned in the text. 1, Observation peatland on Anticosti Island (Lavoie and Filion, 2001; Sauvé, 2016); 2, St. Lawrence Estuary (SLE), COR0602-42PC (Lemay-Tougas, 2014) and MD99-2220 (de Vernal et al., 2013a); 3, COR0503-37PC (Dhahri, 2010; Genovesi et al., 2011); 4, CR06-TCE (Thibodeau et al., 2013); 5, 89-007-111 (de Vernal et al., 1993); 6, Baie-Comeau peatlands (Magnan and Garneau, 2014; Sauvé, 2016); 7, Havre-Saint-Pierre peatlands (Magnan and Garneau, 2014; Sauvé, 2016); 8, Petit Lac Bouchard and 9, Lac du Triangle lake sediments (Asnong and Richard, 2003); 10, Lac à Euloge and Lac J'Arrive lake sediments (Marcoux and Richard, 1995); 11, AI07-04BC/03G, Bonavista Bay (Solignac et al., 2011; Sicre et al., 2014); 12, AI07-11BC/12G, Placentia Bay (Jessen et al., 2011; Solignac et al., 2011; Sicre et al., 2014); 13, 95-030-24 (Levac, 2001); 14, MD99-2225, Bay of Islands (Levac, 2003); 15, MD95-2033 (Balestra et al., 2013); 16, Nordan's Pond Bog (Hughes et al., 2006); 17, Robinsons and Joe's Ponds (McCarthy et al., 1995); 18, Baltic Bog (Peros et al., 2016); 19, Avalon Peninsula (Macpherson, 1982). The map was made with Ocean Data View.

GSL and nearshore Atlantic Canada (Fig. 1). Results indicate important variations of SSTs throughout the Holocene. However, none of the abovementioned records provide a temporal resolution suitable to resolve centennial to decadal variability of hydrographical conditions. In terrestrial areas surrounding the GSL, pollen, spores, and testate amoebae preserved in peat bogs and lake sediments show changes in the vegetation coupled with large variations in water table depth (e.g., McCarthy et al., 1995; Hughes et al., 2006; Magnan and Garneau, 2014; Peros et al., 2016; Sauvé, 2016; Fig. 1), suggesting climate variations accompanied with changes in precipitation regimes.

In this context, we focus on the central part of the GSL with the aim of producing a palynological record of the last 2000 yr with multidecadal resolution. Our study includes the analysis of dinocyst assemblages to reconstruct the natural variations of sea-surface conditions, including temperature, salinity, sea-ice cover, and primary productivity (cf. de Vernal et al., 2001, 2013b, 2020), which are parameters intimately related to climate. Our analyses also include pollen and spores, with the aim of making direct correlation with onshore vegetation history of surrounding lands and establishing linkages between onshore and offshore climate history. The high temporal resolution allows us to capture the events that punctuated the otherwise long-term climate changes. A secondary objective of our study is to evaluate the impact of the ongoing global anthropogenic warming on regional climate. This work adds a new piece of information to document regional climate changes and provides a framework for the climatic conditions or stresses that the Indigenous populations and European migrants have experienced.

REGIONAL SETTING

The GSL covers an area of about 235,000 km^2 and represents 35,000 km^3 of water, including the SLE (Galbraith et al., 2012). The dominant bathymetric feature is the Laurentian Channel, which is over 250 m deep and ~1240 km long. It extends from the southeastern Canadian continental shelf all the way to the mouth of the Saguenay Fjord near Tadoussac (Fig. 1). The circulation in the Laurentian Channel is estuarine, with water flowing seaward in the surface layer, which is about 50 m thick, and landward in the deep layer (Saucier et al., 2003). At greater depths, warm and oxygen-poor North Atlantic Central Water as well as cold and oxygen-rich Labrador Current Water (LCW) intrude through the main channels (Gilbert et al., 2005). At the surface, freshwater runoff from the watershed enters the GSL through the estuary and from rivers of the north shore. The gulf receives about 600 km^3 of freshwater annually, 84% of which is from the St. Lawrence River System (cf. Koutitonsky and Bugden, 1991). Based on annual climatological means of 1981–2010, runoff from the St. Lawrence River and all other major rivers draining into separate gulf regions have a total of 20,852 m^3/s (Galbraith et al., 2019). Because of the large freshwater discharge, the

https://doi.org/10.1017/qua.2021.56 Published online by Cambridge University Press

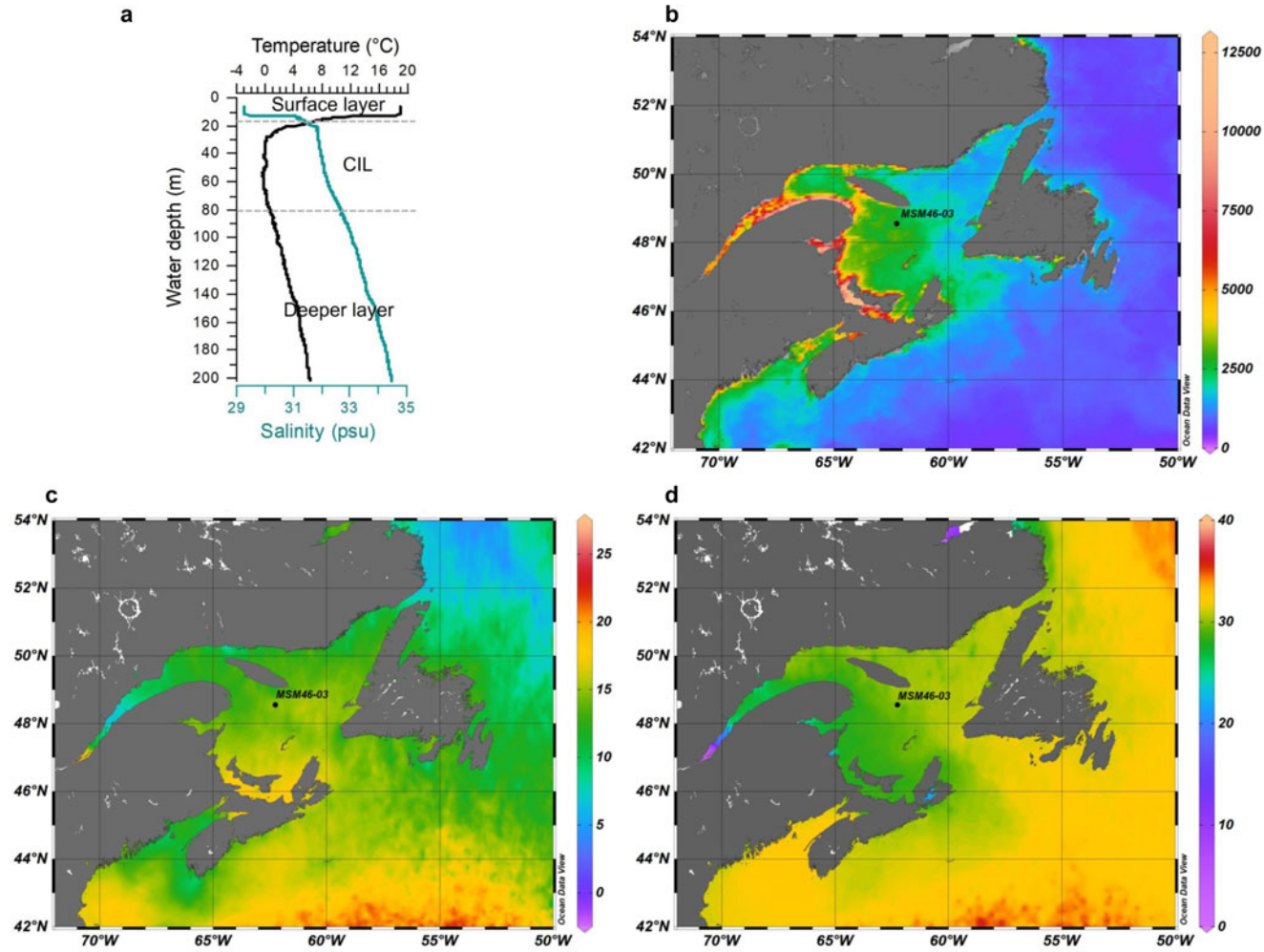

Figure 2. (a) Temperature and salinity profile at site MSM46-03 in August 2015 showing the three water layers: the surface layer, the cold intermediate layer (CIL), and the deeper layer. (b) Map of primary productivity (mgC/m^2/day) in August 2015 based on the standard VGPM algorithm (Behrenfeld and Falkowski, 1997). (c, d) Maps of summer (July–September) temperature (°C) and salinity (psu) at the surface based on 1955–2012 statistical mean (NOAA Northwest Atlantic regional climatology; Seidov et al., 2016).

estuary–gulf system is marked by a pronounced salinity gradient, with surface salinities varying from an annual average of <28 psu at the head of the Laurentian Channel to about 31 psu at the Cabot Strait (Seidov et al., 2016; Fig. 2d). In addition, surface water in the northeast part of the GSL is influenced by LCW that enters the area via the Strait of Belle Isle (see Fig. 2d). The wind regime in eastern Canada is currently governed by the relative strength of three major air masses: the modified mild dry Pacific air mass from the west, the cold dry Arctic air mass from the north and northwest, and the warm moist Atlantic Maritime Tropical air mass from the south (Bryson, 1966; Bryson and Hare, 1974; Fig. 1).

The water column of the GSL is highly stratified, with three distinct layers: the surface layer, the cold intermediate layer (CIL), and the deeper layer (Galbraith et al., 2012; Fig. 2a). The surface waters are characterized by low salinity and relatively high temperature in summer because of mixing with continental runoff, whereas the deep waters that originate from Atlantic and Labrador shelf waters are saltier and colder (Saucier et al., 2003; Gilbert et al., 2005; Galbraith et al., 2012). Surface temperature typically reaches maximal values averaging 15.6°C (1985–2010) from mid-July to mid-August, followed by a gradual cooling and freezing in winter (Galbraith et al., 2019). The surface layer thickens in winter and reaches near-freezing temperatures (−1.8°C to 0°C; Galbraith, 2006).

At the study site, mean summer (July to September) SST and sea-surface salinity (SSS) from 1955 to 2012 are 14.0 ± 2.1°C and 29.3 ± 1.0 psu, respectively (Seidov et al., 2016; Fig. 2c and d). The seasonal duration of sea-ice cover in the central gulf region is 2.5 ± 1.0 months/yr based on the 1985–2010 instrumental data (Galbraith et al., 2019). Upwelling occurs in the GSL at the head of the Laurentian Channel and in coastal areas (e.g., Saucier et al., 2003; Galbraith et al., 2012), contributing to high primary productivity as estimated from satellite data. For example, the estimation of net primary production based on chlorophyll data from the Moderate Resolution Imaging Spectroradiometer (MODIS) program and calculated with the Vertical Generalized Production Model (VGPM; Behrenfeld and Falkowski, 1997) is 311 gC/m^2/yr at the study core site, with mean summer primary productivity of 1897 ± 488 mgC/m^2/day (MODIS R2018 data; Fig. 2b; original data available at http://science.oregonstate.edu/ocean.productivity/index.php).

The GSL area is characterized by a mild, cool, and moist climate due to the proximity of the Atlantic Ocean, with long

https://doi.org/10.1017/qua.2021.56 Published online by Cambridge University Press

winters and relatively short summers (Agriculture and Agri-Food Canada, 2013). According to the 1981–2010 climate data at the four stations closest to the study site (Fig. 1), maximum temperature is reached in July or August with mean summer temperatures of 14.8°C at Cap Des Rosiers, 15.2°C at Doyles, 16.3°C in the Magdalen Islands, and 13.1°C at Natashquan. Mean winter temperatures are −8.1°C, −4.9°C, −6.2°C, and −11.7°C at the above stations, respectively. Annual precipitation is exceptionally high at Doyles, averaging 1505 mm. Elsewhere, it ranges between 1037 and 1195 mm.

In the surrounding land, the regional climate results in the development of coniferous forests of the Northern Forests ecoregion in the north and mixed conifer-hardwood forests of the Eastern Temperate Forests ecoregion in the southwest (e.g., Commission for Environmental Cooperation, 1997; Fig. 1). In the north, cool climate, short growing season, and frequent forest fires result in a forest vegetation dominated by balsam fir (*Abies balsamea*), black spruce (*Picea mariana*), white spruce (*Picea glauca*), and paper birch (*Betula papyrifera*). Jack pine (*Pinus banksiana*) is rare, and white pine (*Pinus strobus*) is present on Anticosti Island but not abundant. The forests are often mixed with bogs, marshes, and other wetlands. Southwest of the GSL, the vegetation is characterized by a mixture of coniferous and deciduous trees. In addition to firs, spruces, and birches, thermophilic trees like maple (*Acer*), hemlock (*Tsuga*), and beech (*Fagus*) are found in the forest. White pine is more frequent, and jack pine is still rare.

MATERIALS AND METHODS

The study sequence includes a 36-cm-long multicore and a 901-cm-long gravity core from site MSM46-03 (48°33.02′N, 62° 14.95′W; water depth = 449 m) in the Laurentian Channel. The internal diameters of the multicorer and the gravity corer are 10 and 12 cm, respectively. The multicore device that penetrates the seafloor slowly yields undisturbed samples of surface sediment, while the gravity core allows recovery of deeper sediments. The cores were collected during the *Maria S. Merian* expedition MSM 46 in August 2015 (Pollehne, 2015). The seismic profile and previous studies of a nearby site show that the coring location is characterized by high sedimentation rate suitable for our study, which requires high temporal resolution (Cauchon-Voyer et al., 2005). The sediments consist mostly of light olive gray silty clay with black faint sulfidic layers occurring throughout the upper 143 cm of the gravity core. The sulfidic layers indicate reducing environments that are generally rich in organic material. The core sediment was subsampled at 1-cm intervals. The total organic carbon was calculated from the difference between the total carbon and the toral inorganic carbon concentrations (see Supplementary Material 1 for detail).

Chronology

The chronology of the multicore MSM46-03-05-MUC3 and the gravity core MSM46-03-12-GC was established based on accelerator mass spectrometry (AMS) ^{14}C dates, 1 in the multicore and 22 in the gravity core (Table 1). The interval from 69 to 74 cm in the gravity core has been excluded due to redeposition, as it consists of a sandy layer, and the radiocarbon date from this depth indicates age reversal (Table 1). The AMS radiocarbon dates were calibrated using the Marine13 calibration curve (Reimer et al., 2013). A correction for marine reservoir effect was estimated from the database of Reimer and Reimer (2001) and McNeely et al. (2006). This yielded delta *R* (Δ*R*) values of 246 ± 169 yr, in addition to the conventional 400 yr of air–sea reservoir difference. To establish independent age–depth relationships in both cores, we used the Bacon package (Blaauw and Christen, 2011) available on the R interface (R Development Core Team, 2013). Bacon uses Bayesian statistics to reconstruct accumulation histories for deposits through a high number of Markov chain Monte Carlo iterations. The age model indicates that the upper 520 cm of the gravity core encompasses the last ~8500 yr with sedimentation rates of 0.3–1.7 mm/yr (Fig. 3c). In this study, we focus on the upper 230 cm of the gravity core, which spans the last two millennia. Sedimentation rate averages 1.4 mm/yr in this section.

Percentages of two dominant dinocyst taxa, *Pentapharsodinium dalei* and *Islandinium minutum*, were used to correlate the multicore and the top of the gravity core (Fig. 3b). The correlation suggests an overlap between the two cores and a missing layer of about 13 cm at the top of the gravity core. Hence, we were able to create a composite sequence at site MSM46-03 with a continuous chronology from 1700 to –65 cal yr BP (250 to 2015 CE). The transition from the multicore record to the gravity core record was made at 13 cm in the gravity core.

Palynological analysis

In the multicore, which encompasses ~300 yr, the palynological analyses were performed at 2 cm intervals in the upper 9 cm and at 4 cm intervals below, which provides a multidecadal time resolution. In the gravity core, the upper 230 cm generally was analyzed at 4 cm intervals, which provides a temporal resolution of 10 to 40 yr (see Supplementary Table 1 for details on sampling depths).

Samples were processed for palynological analyses according to the protocol described by de Vernal et al. (1999). See also Supplementary Material 1 for details. Because the sediment contains abundant organic debris, we used a solution of KOH to deflocculate the fine sediment. Such treatment, which oxidizes organic matter, is usually avoided for isolation of dinocysts, because some taxa, notably the cysts of protoperidiniales, could be damaged (e.g., Zonneveld et al., 2008). Hence, we used a very gentle treatment with 5% KOH for 10 to 15 minutes. We tested this treatment to ensure the preservation of dinocysts. Four samples were treated with and without KOH. As presented in Supplementary Table 2, there is no evidence for reduction of dinocyst concentration or selective oxidation of certain species. The identification and counting of common palynomorphs were made under an optical microscope with transmitted light at magnifications of 400× and 1000×. We routinely identified most palynomorphs, which include pollen grains, spores, dinocysts, and organic linings of benthic foraminifera. We also counted what we interpret to be reworked palynomorphs based on their identification and preservation states. The detailed counts are presented in Supplementary Table 1.

One *Lycopodium clavatum* spore tablet per sample was added before chemical and mechanical treatments for further estimation of the absolute abundances of palynomorphs (e.g., Faegri and Iversen, 1964). A minimum of 300 specimens of dinocysts were counted in each sample to provide statistically reliable counts (e.g., Mertens et al., 2009). Relative abundances of dinocyst taxa are presented as percentages of the total number of counted dinocyst specimens (Figs. 4 and 5). The number of pollen grains counted ranges from 300 to 500 and that of spores ranges from

https://doi.org/10.1017/qua.2021.56 Published online by Cambridge University Press

Table 1. Accelerator mass spectrometry (AMS) radiocarbon dates of multicore MSM46-03-05-MUC3 and gravity core MSM46-03-12-GC with corresponding calibrated ages.[a]

Lab ID[b]	Sample depth (cm)	Dated material	^{14}C date (yr BP)	ΔR (yr)	Calibrated age range (±1σ)	Mean age (cal yr BP)
MSM46-03-05-MUC3						
AWI-5609.1.1	17.5	Mollusk	677 ± 72	246 ± 169		
MSM46-03-12-GC						
AWI-5610.1.1	5.5	Mix of mollusk, ostracod valves and benthic foraminifera	748 ± 77	246 ± 169	0–260	190
ETH-87298	8.5	Mollusk	715 ± 50	246 ± 169	0–236	133
ETH-87299	19.5	Mixed benthic foraminifera	845 ± 50	246 ± 169	69–384	227
ETH-87301	39.5	Mixed benthic foraminifera	915 ± 40	246 ± 169	139–461	300
ETH-94424	51.5	Mixed benthic foraminifera	1005 ± 45	246 ± 169	230–548	389
ETH-88835	60.5	Mollusk	1305 ± 50	246 ± 169	487–791	639
ETH-64526	69.5	Mixed benthic foraminifera	1760 ± 60	246 ± 169	902–1255	1065
ETH-88836	79.5	Mixed benthic foraminifera	1190 ± 50	246 ± 169	386–692	539
ETH-88837	99.5	Mixed benthic foraminifera	1490 ± 50	246 ± 169	637–961	799
AWI-5611.1.1	111.5	Mixed benthic foraminifera	1443 ± 76	246 ± 169	598–929	770
ETH-87302	119.5	Mixed benthic foraminifera	1540 ± 50	246 ± 169	667–1004	836
ETH-94425	126.5	Mollusk	1540 ± 50	246 ± 169	667–1004	836
ETH-94426	142	Mixed benthic foraminifera	1845 ± 50	246 ± 169	955–1307	1131
ETH-87303	169.5	Mixed benthic foraminifera	1930 ± 50	246 ± 169	1037–1411	1224
AWI-5612.1.1	176.5	Mixed benthic foraminifera	1763 ± 77	246 ± 169	897–1263	1068
ETH-94427	189.5	Mixed benthic foraminifera	2045 ± 50	246 ± 169	1172–1546	1359
ETH-94428	209.5	Mixed benthic foraminifera	2110 ± 50	246 ± 169	1244–1617	1431
ETH-64527	219.5	Mixed benthic foraminifera	2365 ± 55	246 ± 169	1503–1915	1707
ETH-94429	241	Mixed benthic foraminifera	2460 ± 50	246 ± 169	1595–2020	1808
AWI-5613.1.1	266	Mixed benthic foraminifera	2509 ± 82	246 ± 169	1648–2105	1878
ETH-87304	269.5	Mixed benthic foraminifera	2575 ± 50	246 ± 169	1723–2157	1940
ETH-64528	369.5	Mixed benthic foraminifera	4360 ± 60	246 ± 169	3923–4406	4169
ETH-64529	519.5	Mixed benthic foraminifera	8385 ± 70	246 ± 169	8422–8807	8663

[a]The calibration data set was Marine13 (Reimer et al., 2013).
[b]Laboratory codes: AWI, MICADAS laboratory at Alfred Wegener Institute; ETH, ETH Zurich. The shaded radiocarbon date was excluded due to redeposition from 69 to 74 cm in the gravity core.

10 to 60 per sample. The results are presented as percentages of the pollen taxa versus the total number of pollen grains, and the percentages of spore taxa are reported versus the total number of spores (Figs. 4 and 6). All results are reported in Supplementary Table 3. The taxonomic nomenclature of dinocysts was mainly based on Rochon et al. (1999) and Radi et al. (2013). Pollen grains and spores were identified mainly based on the atlases and identification keys of Richard (1970) and McAndrews et al. (1973). Distinction between pollen grains of *Betula* tree and *Betula* shrub was based on grain size. *Betula* grains > 20 µm were classified as *Betula* tree and those < 20 µm as *Betula* shrub (cf. Mudie, 1982; Mäkelä, 1996).

Quantitative treatment and reconstruction of sea-surface conditions

Multivariate analysis was performed on dinocyst data as well as pollen data using CANOCO 5 software (ter Braak and Šmilauer, 2012) to help define zonations. A square-root transformation was applied to dinocyst taxa abundances to reduce the effect of very dominant taxa, while logarithmic transformation was applied to pollen taxa abundances to obtain higher explained variation by the first two components. Occasional taxa found in low numbers and in less than five samples were excluded from the analysis. Sample scores for the first (PC1) and second (PC2) principal components are reported in Supplementary Table 3. Each principal component axis has an eigenvalue expressed as a percentage that represents the amount of variation explained by the axis.

The sea-surface parameters, including summer SSS, summer SST, sea-ice cover, and summer productivity, were reconstructed from dinocyst data using the modern analog technique (MAT; cf. Guiot and de Vernal, 2007). The software package developed by Guiot in the R environment (http://cran.r-project.org) and the latest modern dinocyst database (de Vernal et al., 2020) were used to perform the MAT. The database includes

https://doi.org/10.1017/qua.2021.56 Published online by Cambridge University Press

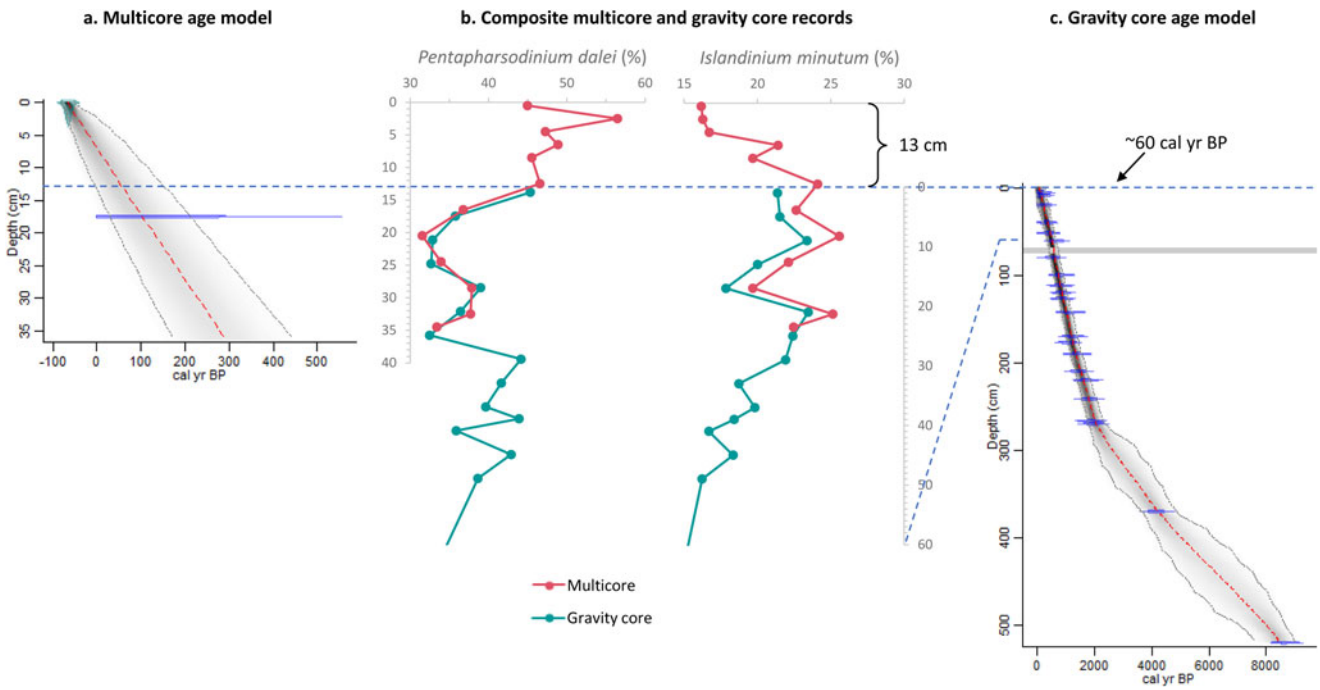

Figure 3. Composite sequence and age vs. depth relationship in the multicore and the gravity core at site MSM46-03. The age models are based on ^{14}C dates in (a) the multicore MSM46-03-05-MUC3 and (c) the gravity core MSM46-03-12-GC using Bacon software (Blaauw and Christen, 2011). Calibrated age ranges are shown in semi-transparent blue. The semi-transparent blue-green symbol at the top of part a corresponds to the coring date (2015 CE). Grayscales indicate probability, where darker gray indicates more likely ages. Red dashed line represents median values, and gray dashed lines represent 95% confidence ranges. The horizontal gray zone in part c represents the redeposition zone from 69 to 74 cm in the gravity core. (b) Curves of *Pentapharsodinium dalei* and *Islandinium minutum* percentages allow establishment of the correlation between the multicore and the gravity core.

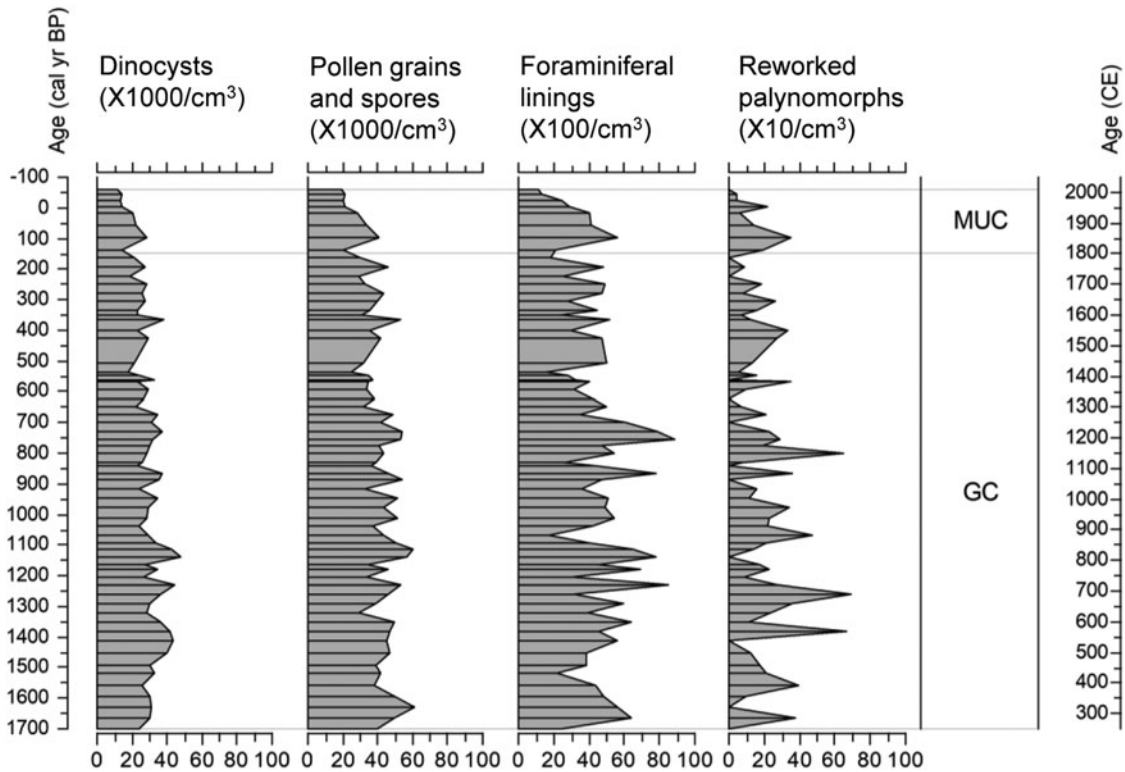

Figure 4. Concentrations of dinocysts; pollen grains and spores; organic foraminiferal linings; and reworked palynomorphs (number of specimens/cm^3 of sediment) in composite sequence MSM46-03. MUC, multicore; GC, gravity core.

https://doi.org/10.1017/qua.2021.56 Published online by Cambridge University Press

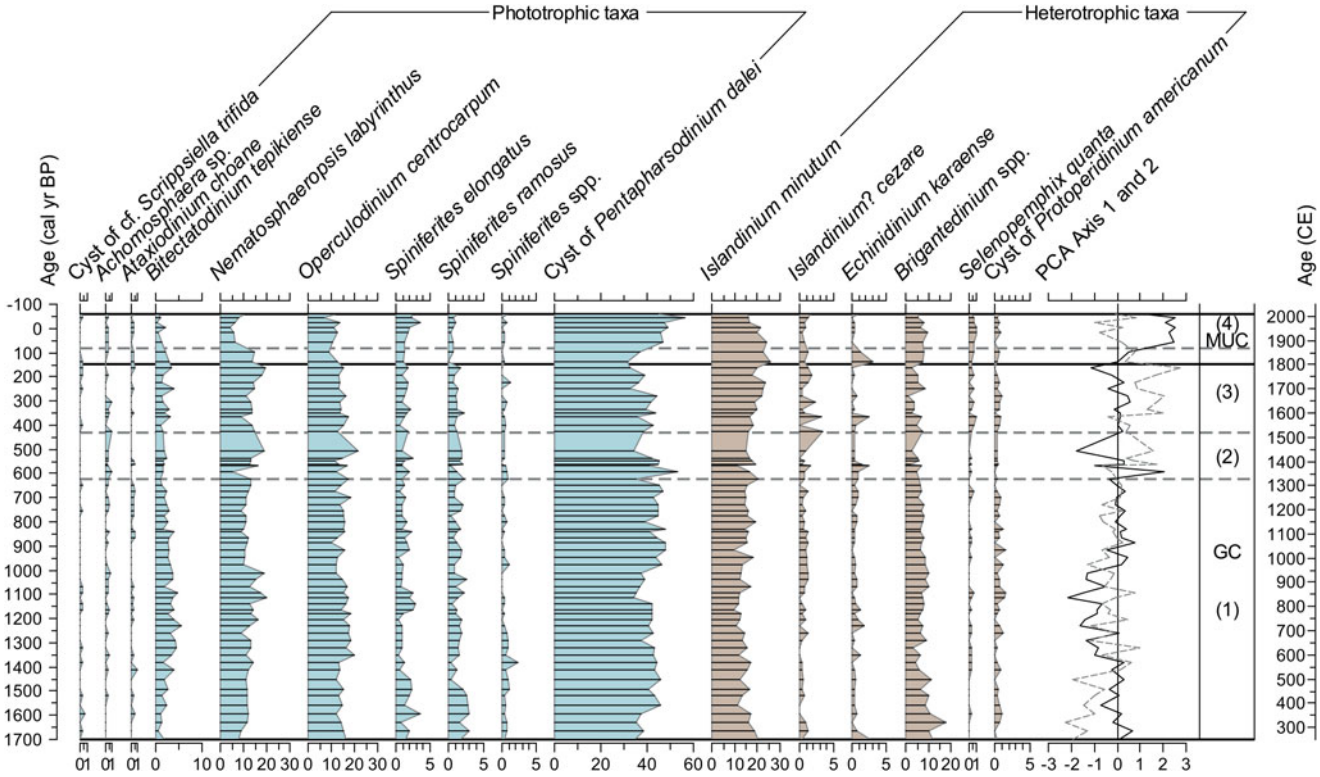

Figure 5. Percentages of the main dinocyst taxa and stratigraphic plot of principal component analysis (PCA) axis 1 (black solid line) and axis 2 (gray dashed line) sample scores in composite sequence MSM46-03. MUC: multicore; GC: gravity core. Horizontal gray dashed lines and numbers in brackets indicate zones defined by PCA scores mentioned in the text.

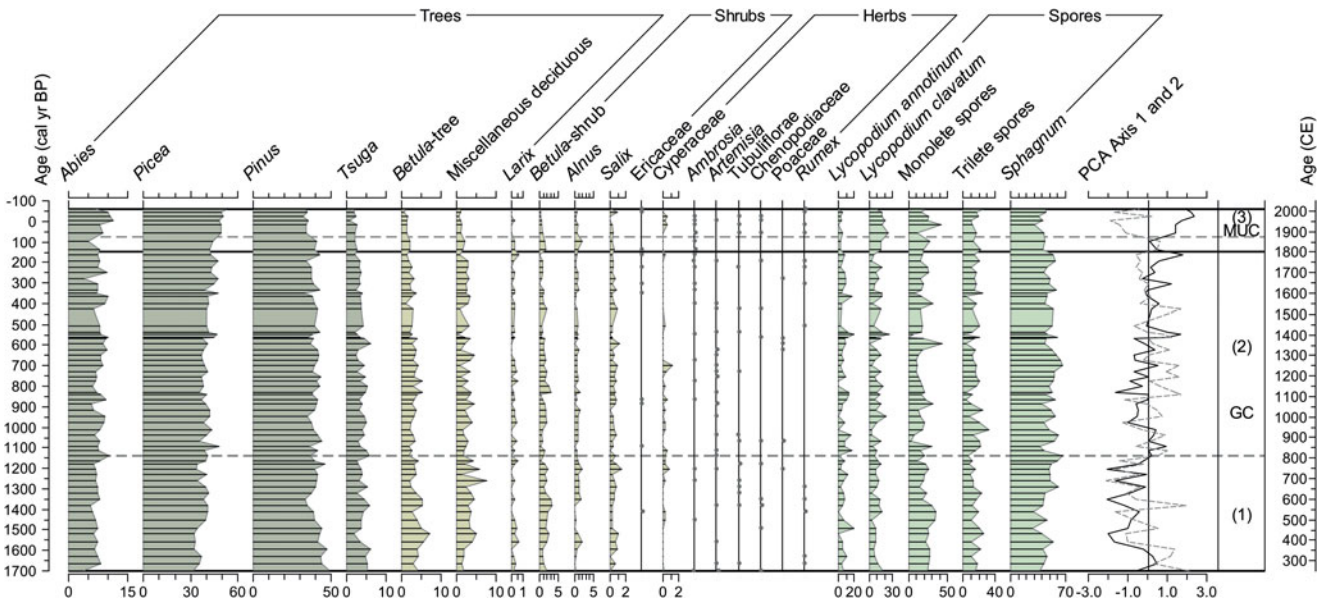

Figure 6. Percentages of pollen and spore taxa and stratigraphic plot of principal component analysis (PCA) axis 1 (black solid line) and axis 2 (gray dashed line) sample scores for the pollen assemblages in composite sequence MSM46-03. MUC, multicore; GC, gravity core. Horizontal gray dashed lines and numbers in parentheses correspond to zones defined by PCA scores. Pollen percentages and spore percentages were calculated on the pollen sum and spore sum, respectively. For some rare (<1%) and occasional taxa, occurrence is indicated by a dot. *Betula* trees correspond to pollen grains larger than 20 μm and vice versa for *Betula* shrubs. Miscellaneous deciduous taxa include *Acer*, *Quercus*, *Carpinus*/*Ostrya*, *Corylus*, *Carya*, *Castanea*, *Fraxinus*, *Juglans*, *Tilia*, and *Ulmus*. Trilete spores include those other than *Lycopodium* and *Sphagnum*.

abundances of 71 dinocyst taxa at 1968 sites across the Northern Hemisphere. A validation test yielded root-mean-square error of prediction of ±1.9 psu for summer SSS, ±1.9°C for summer SST, ±1.5 months/yr for sea-ice cover, and ±653 mgC/m^2/day for summer productivity. The distance of the modern analogs is used as an indicator of the reliability of the analogs. In the case

https://doi.org/10.1017/qua.2021.56 Published online by Cambridge University Press

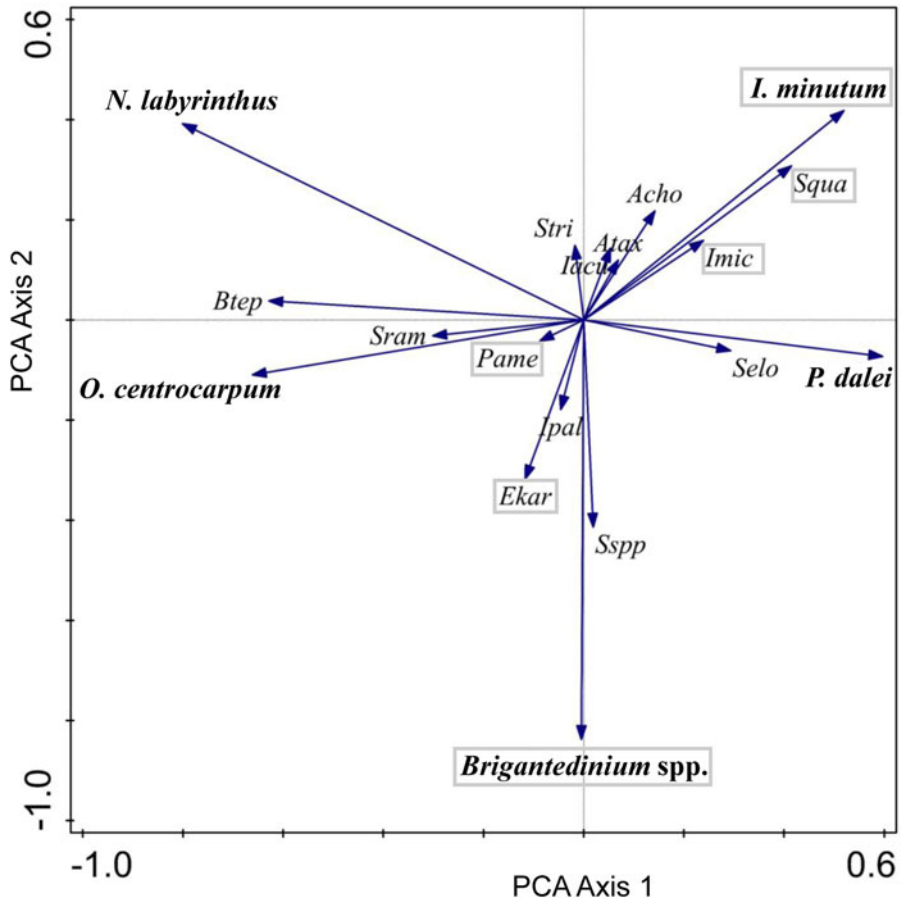

Figure 7. Ordination diagram of the dinocyst taxa from MSM46-03 cores. Principal component analysis (PCA) axis 1 eigenvalue = 17.8%; PCA axis 2 eigenvalue = 13.5%. Taxa are indicated by species name for dominant taxa and by four-letter abbreviations for the others (*Imic*, *Islandinium*? *cezare*; *Stri*, cyst of cf. *Scrippsiella trifida*; *Btep*, *Bitectatodinium tepikiense*; *Pame*, cyst of *Protoperidinium americanum*; *Ipal*, *Impagidinium pallidum*; *Squa*, *Selenopemphix quanta*; *Ekar*, *Echinidinium karaense*; *Iacu*, *Impagidinium aculeatum*; *Acho*, *Achomosphaera* sp.; *Atax*, *Ataxiodinium choane*; *Selo*, *Spiniferites elongatus*; *Sram*, *Spiniferites ramosus*; *Sspp*, *Spiniferites* spp.) Heterotrophic taxa are distinguished from phototrophic taxa by gray boxes around their names.

of the n = 1968 database, the threshold distance for analog after log transformation of the taxa occurrences is 1.2.

Pollen grains and spores in marine sediments such as those of the GSL originate from distal sources through eolian and fluvial transports (de Vernal and Giroux, 1991). Therefore, we did not attempt quantitative reconstructions of climate parameters.

RESULTS

Palynological assemblages

Pollen grains and spores are the most abundant palynomorphs in the samples (~40,000 grains/cm^3; Fig. 4; Supplementary Table 4). Dinocysts are slightly less abundant, with concentrations around 30,000 cysts/cm^3. Foraminiferal lining concentrations fluctuate around 5000 linings/cm^3. Reworked palynomorph concentrations are low, ranging from 0 to 700/cm^3. Concentrations of pollen grains and spores, dinocysts, foraminiferal linings, and reworked palynomorphs are relatively stable throughout the record.

The total organic carbon content averages 1.8% in the section analyzed. From sedimentation rates that average 1.4 mm/yr, we calculate fluxes of the order of 10^3 dinocysts/cm^2/yr, which represents high fluxes as compared with many regions of the Northern Hemisphere (de Vernal et al., 2020). Together, the high organic carbon content and the dinocyst fluxes suggest high pelagic production.

Dinocyst assemblages

Cysts of *P. dalei*, *I. minutum*, *Operculodinium centrocarpum*, *Nematosphaeropsis labyrinthus*, and *Brigantedinium* spp. are the dominant taxa throughout the record (Fig. 5). The assemblages indicate a temperate environment, with a high seasonality of temperature, as suggested by the occurrence of both warm SST-related and sea ice–related taxa. For example, *Bitectatodinium tepikiense* occurs mostly at mid-latitudes of the North Atlantic but tolerates freezing winter conditions; it is more abundant where summer temperatures are higher than 10°C (Rochon et al., 1999; de Vernal and Marret, 2007; de Vernal et al., 2020). *Islandinium* spp. are shown to occur in areas characterized by seasonal sea-ice cover (e.g., Rochon et al., 1999; de Vernal et al., 2013a). In addition, the relatively high species diversity of the dinocyst assemblage together with the dominance of phototrophic taxa such as *P. dalei*, *O. centrocarpum*, and *N. labyrinthus* suggests a high primary productivity, as commonly observed in productive environments from the North Atlantic (cf. de Vernal and Marret, 2007).

Multivariate analyses were performed on dinocyst data to characterize patterns of variation in the occurrence of 18 main taxa (Fig. 7). Response data have a gradient of 0.6 SD units long, so linear method and principal component analysis (PCA) is recommended (ter Braak and Šmilauer, 2012). The first and second axes explain 17.8% and 13.5% of the variance, respectively. PC1 is marked by a strong opposition between some phototrophic species (*O. centrocarpum*, *B. tepikiense*, *N. labyrinthus*, *Spiniferites ramosus*) on the negative side and *Islandinium*? *cezare*, *Spiniferites elongatus*, *Islandinium minutum*, *Selenopemphix quanta*, and *P. dalei* on the positive side. PC2 shows high scores of *N. labyrinthus* and *I. minutum* on the positive side, opposed to *Brigantedinium* spp., *Spiniferites* spp., and *Echinidinium karaense* on the negative side.

https://doi.org/10.1017/qua.2021.56 Published online by Cambridge University Press

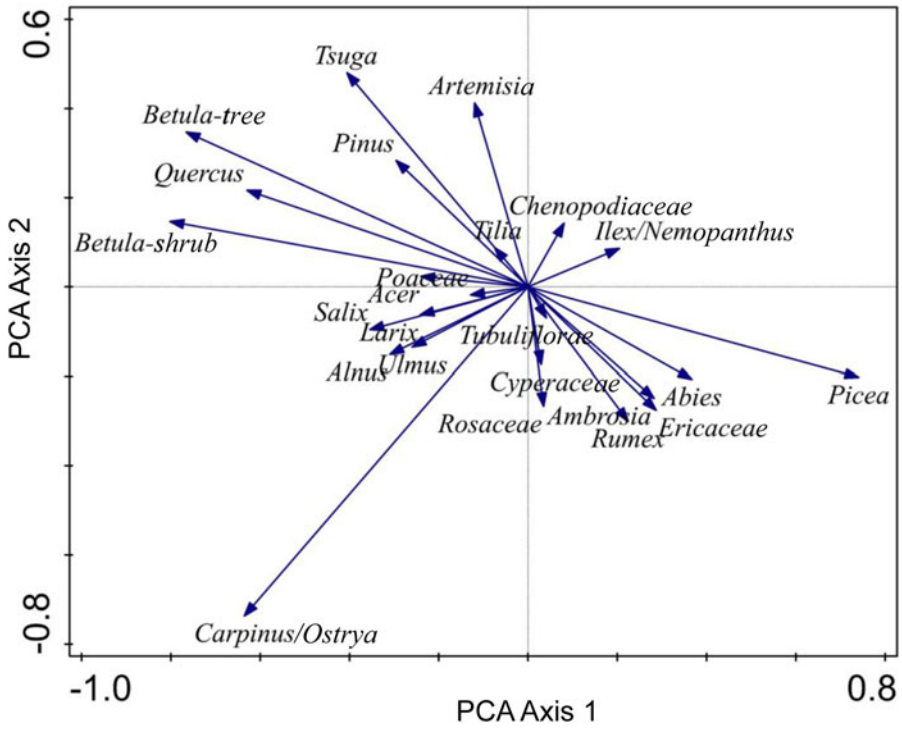

Figure 8. Ordination diagram of the pollen taxa from cores MSM46-03. Principal component analysis (PCA) axis 1 eigenvalue = 29.6%; PCA axis 2 eigenvalue = 13.7%.

The stratigraphic plot of PC1 and PC2 sample scores helped to define assemblage zones. Zone 1 represents the interval before about 625 cal yr BP (1325 CE). It is characterized by generally negative or low values of both PC1 and PC2. This is related to high percentages of *Brigantedinium* spp., *Spiniferites* taxa, *P. dalei*, and *B. tepikiense* and low percentages of *Islandinium*. After 625 cal yr BP (1325 CE) and before 430 cal yr BP (1520 CE), the assemblages are unstable, as shown by PC1 and PC2 fluctuations, which characterize zone 2. In zone 3, from 430 to 80 cal yr BP (1520–1870 CE), high PC2 scores are recorded with low percentages of *Brigantedinium* spp. relative to high percentages of *Islandinium*. Finally, zone 4, spanning from 80 cal yr BP to the present (1870–2015 CE) is marked by highly positive PC1 values and negative PC2 values, which correspond to an increase of *P. dalei* and *S. elongatus* percentages and a decrease of *Islandinium*, *N. labyrinthus*, and *B. tepikiense*.

Pollen and spore assemblages

Pollen assemblages are dominated by conifer taxa, including *Picea*, *Pinus*, and *Abies* (Fig. 6). They are accompanied by the conifer *Tsuga* and a deciduous taxon *Betula* in relatively high percentages (1%–7%). In addition to *Betula*, miscellaneous deciduous taxa include predominantly *Acer*, *Quercus*, *Carpinus*/*Ostrya*, and rarely, *Carya*, *Castanea*, *Fraxinus*, *Juglans*, *Tilia*, and *Ulmus*. Some shrub taxa, including *Betula*, *Alnus*, *Salix*, and *Corylus*, are present, while herb taxa are rare, the most frequent one being Cyperaceae. The spores are dominated by *Sphagnum*. The pollen data are compatible with inputs from the coniferous-hardwood forest vegetation in lands surrounding the GSL. The record is characterized by increasing *Picea* pollen percentages, relative to the decrease of *Pinus* and *Tsuga* and pollen of deciduous trees, including *Betula*, over the last 1700 yr.

PCA was performed based on the percentages of the 24 main pollen taxa (Fig. 8). Response data have a gradient of 0.7 SD units long, suggesting that a linear method such as PCA is appropriate. PC1 and PC2 explain 29.6% and 13.7% of the variance, respectively. PC1 is characterized by a strong opposition between *Picea* on the positive side and pollen of deciduous tree species (*Betula*, *Quercus*, *Carpinus*/*Ostrya*) on the negative side. PC2 is characterized by a large distance between *Carpinus*/*Ostrya* and other taxa.

Three main assemblage zones can be distinguished. In zone 1, corresponding to the interval before 1140 cal yr BP (810 CE), low values of PC1 and PC2 correspond to low percentages of *Picea* and high percentages of deciduous tree taxa in the assemblages. In zone 2, spanning a large part of the last millennium (~810–1880 CE), scores of PC1 and PC2 fluctuate around 0 together with a slight increase of PC1 as the result of gradual increase of *Picea* relative to pollen of other conifers (*Pinus*, *Tsuga*) and deciduous trees (e.g., *Betula*). Finally, in zone 3, which corresponds to the most recent interval, from ~1880 to 2015 CE, PC1 continued to increase, but PC2 scores were significantly lower than in zone 2, which corresponds to an increase of *Abies* relative to a rapid decrease of *Pinus* percentages.

Reconstruction of sea-surface conditions

The reconstruction of sea-surface parameters (Fig. 9) from dinocyst data yielded estimates that we consider as reliable as possible according to the criteria proposed by de Vernal et al. (2013a): (1) the counted dinocyst sums were all above 300; and (2) the distance of the analogs ranged from 0.1 to 0.5 and never exceeded 0.6, which is well below the threshold of 1.2.

Reconstructed summer SST ranges from 6°C to 14°C with a maximum between 1590 and 1230 cal yr BP (360–720 CE) of 12°C to 14°C, which is close to modern values. This warm phase corresponds to 2–2.5 months of sea-ice cover in winter, summer SSSs of 30–30.5 psu, and summer primary productivity of more than 1500 mgC/m^2/day. After this warm phase, the dinocyst-based reconstruction suggests that there was a shift

https://doi.org/10.1017/qua.2021.56 Published online by Cambridge University Press

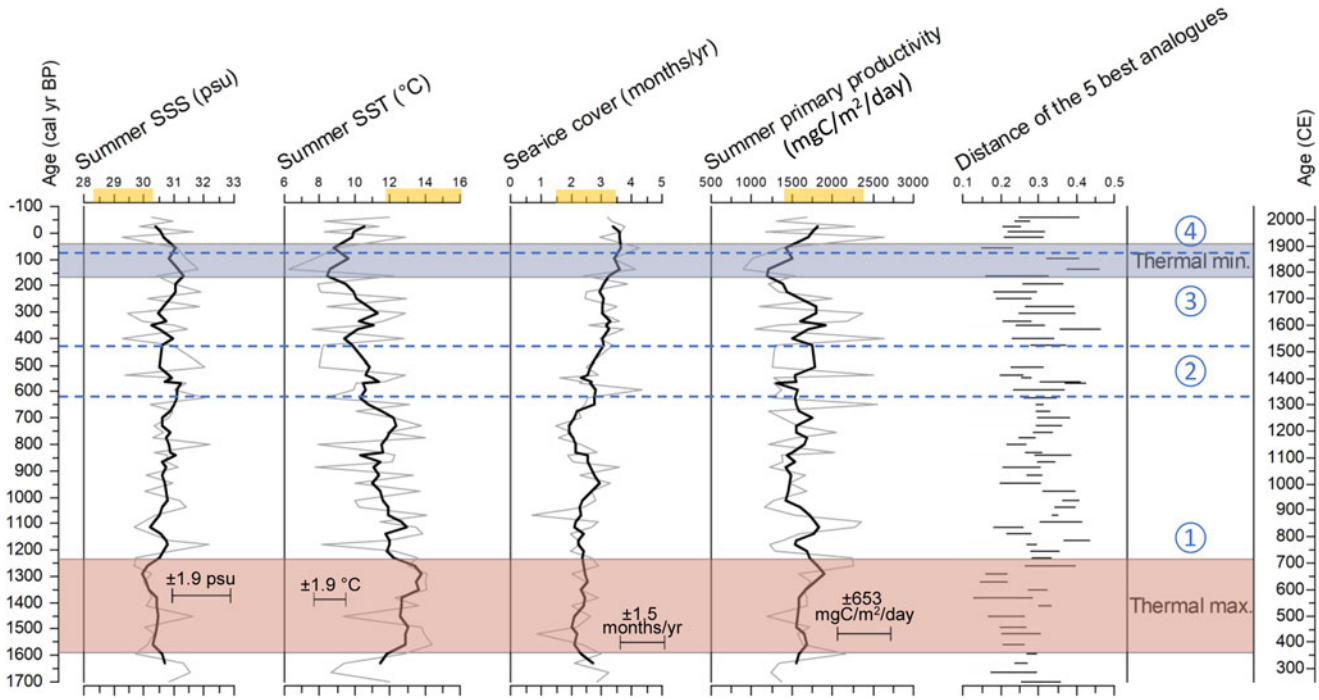

Figure 9. Reconstructed summer sea-surface salinity (SSS), summer sea-surface temperature (SST), sea-ice cover, and summer primary productivity (gray curves) from dinocyst assemblages in the composite sequence MSM46-03, and distance of the five closest analogs. Bold black curves represent smoothed values over a window of five consecutive data points. Horizontal red and blue bands correspond to climate intervals mentioned in the text in reference to reconstructions, while dashed lines correspond to the transitions established from the principal component analysis (PCA; see Figs. 5 and 6). Yellow zones on the upper axis represent modern average values of each parameter (SST, SSS: 1955–2012; sea-ice cover: 1985–2010; primary productivity: 2002–2019). The bars indicate error of prediction from the modern analog technique (MAT; see "Materials and Methods").

toward cooler conditions, with summer SSTs gradually decreasing to ~9°C on the average. This long-term cooling was interrupted by a brief event of warm summer SSTs (>12°C) and short winter sea-ice seasons (< 2 months/yr) around 750 cal yr BP (1200 CE). A particularly cold pulse is recorded from 170 to 40 cal yr BP (1780–1910 CE). It was accompanied by increased winter sea-ice duration up to 4 months/yr and decreased primary productivity to values as low as 900 mgC/m^2/day, while SSSs reached 31.8 psu.

The record of the last century suggests warming of surface waters in summer, increasing primary productivity, and a decrease of SSS. This corresponds to a gradual shift toward modern values. This record is characterized by antiphase variations of summer SSS and SST.

DISCUSSION

Comparison of marine and terrestrial pollen records

The pollen assemblages of our marine record spanning the last 2000 yr are dominated by conifer taxa, including *Pinus* and *Picea* (30%–50%) in addition to *Abies* (5%–10%), while *Betula* is rare (<10%). Such an assemblage differs from terrestrial pollen records of the north shore of the GSL, which are typically dominated by *Picea* and *Betula* (30%–50%) with a low proportion of *Pinus* (<10%) (Lavoie and Filion, 2001; Sauvé, 2016; Fréchette et al., 2021; Fig. 1, nos. 1, 6, 7). In Gaspésie and southwestern Newfoundland, pollen assemblages are also dominated by *Betula* (50%), whereas *Pinus* and *Picea* are rare (<10%) (Marcoux and Richard, 1995; McCarthy et al., 1995; Asnong and Richard, 2003; Fig. 1, nos. 8, 9, 10, 17). On the Avalon Peninsula, southeastern Newfoundland, pollen assemblages are dominated by *Betula* (50%), while *Picea* is relatively abundant (20%) and *Pinus* very rare (<5%) (Macpherson, 1982; Fig. 1, no. 19). Hence, the comparison of our marine pollen data with the regional pollen records shows some discrepancies, notably concerning the percentages of *Pinus*, which is overrepresented, whereas *Betula* is underrepresented. An overrepresentation of bisaccate pollen grains in marine sediments is frequent, and *Pinus* pollen has often been reported as preferentially transported by wind (e.g., Rochon and de Vernal, 1994), while the abundance of *Betula* pollen tends to decrease rapidly offshore (Mudie, 1982).

The GSL is in a region of mixing air masses, with modified mild dry Pacific winds from the west, cold dry Arctic air from the north and northwest, and warm moist tropical maritime air from the south (Bryson, 1966; Bryson and Hare, 1974). Hence, the high proportion of *Pinus* pollen in the study core is probably related to atmospheric inputs from the eastern temperate forest (see Fig. 1), where white pine is abundant (cf. Gilliam et al., 2011). Other marine pollen records from the SLE (Lemay-Tougas, 2014; Fig. 1, no. 2), the Bay of Islands off western Newfoundland (Levac, 2003; Fig. 1, no. 14), and the Placentia Bay of southeastern Newfoundland (Jessen et al., 2011; Fig. 1, no. 12) are consistent with *Pinus* pollen fluxes related to air-mass trajectories. The pollen assemblages of the Placentia Bay exposed to southerly winds from the North Atlantic are dominated by *Pinus* (30%–40%; Jessen et al., 2011), despite its low occurrence in records from adjacent terrestrial sites (Macpherson, 1982). In contrast, the pollen assemblages from the SLE and Bay of Islands core sites, which are nearshore, record relatively high *Betula* percentages (20%–30%) and therefore appear comparable

https://doi.org/10.1017/qua.2021.56 Published online by Cambridge University Press

to nearby terrestrial pollen records (McCarthy et al., 1995; Fréchette et al., 2021).

Interpreting offshore pollen assemblages in terms of atmospheric inputs leads us to suggest that the decreasing percentages of *Pinus* pollen at our study site over the last 2000 yr result from the decaying dominance of the Atlantic Maritime Tropical air mass over other air masses. This could be due to an atmospheric circulation that allowed more frequent incursions of Arctic air masses, which in turn may be the origin of the cooling reconstructed from regional paleoclimatic proxies, including pollen records (cf. O'Brien et al., 1995; Viau et al., 2002; Jessen et al., 2011; Pratte et al., 2017; Fréchette et al., 2021).

Regional vegetation history and hydroclimatic conditions

The pollen record of the last two millennia shows that regions surrounding the GSL were occupied by mixed coniferous-hardwood forests communities, which have developed during the Early to Mid-Holocene (Fréchette et al., 2021). The establishment of the closed forests are documented in the regional terrestrial pollen records mentioned earlier (e.g., Marcoux and Richard, 1995; McCarthy et al., 1995; Lavoie and Filion, 2001; Asnong and Richard, 2003; Sauvé, 2016). The Late Holocene expansion of balsam fir and spruce populations has been inferred from the synchronous increase of their pollen percentages at these terrestrial sites. Such a trend is also seen in our marine pollen record, with *Picea* increasing from 30% to 50% and *Abies* increasing from 5% to 10%. This may be a response of the vegetation to regional climate cooling, as proposed by Anderson (1985) and Fréchette et al. (2021). In eastern Gaspésie, located west of our coring site, a decrease of thermophilic species such as *Pinus strobus* (white pine) and *Betula alleghaniensis* (yellow birch) was also highlighted by Asnong and Richard (2003), who attributed these changes to a trend toward cooler and moister conditions. However, based on increased charcoal abundances, Carcaillet and Richard (2000) suggested that relatively dry summers after 2500 cal yr BP fostered more frequent and severe forest fires in eastern Canada. Although counterintuitive, higher soil moisture does not necessarily relate to higher precipitation, as evapotranspiration is reduced under cool climate conditions (cf. Lavoie and Filion, 2001). The hypothesis of a cooling trend without increasing precipitation is supported by our reconstructions, which illustrate SST decrease in surface waters of the central gulf region together with a slight increase of salinity from 1600 cal yr BP to about 100 yr ago. An increase of summer SSS suggests lower freshwater discharge, thus lower precipitation at the scale of the watershed.

Regional changes in sea-surface conditions

The warm interval of the first millennium of the Common Era until 625 cal yr BP (1325 CE)

This interval that corresponds to the dinocyst zone 1 as defined from PCA is characterized by relatively high percentages of *S. ramosus*, *Spiniferites* spp., and *B. tepikiense*, and by low percentages of *Islandinium*, which together point to relatively warm conditions. The MAT reconstructions suggest summer SST ranging from 11°C to 14°C and sea-ice cover of 2–2.5 months/yr, with the warmest conditions characterizing the 1590 to 1230 cal yr BP interval.

Previous reconstructions based on dinocyst records from the area also revealed relatively warm conditions between 2100 and 1250 cal yr BP in the SLE (Lemay-Tougas, 2014; Fig. 1, no. 2) and until 1000 ^{14}C yr BP at the Bay of Islands off west Newfoundland (Levac, 2003; Fig. 1, no. 14). Similarly, palynological records from Bonavista Bay off northeast Newfoundland (Fig. 1, no. 11) show a maximum of *B. tepikiense* percentages from 1700 to 1100 cal yr BP, suggesting warm summer conditions; in contrast, the Placentia Bay data from southeast Newfoundland (Fig. 1, no. 12) suggest that the warmest period occurred before 1500 cal yr BP, which is earlier than other regional records. However, this is inferred from *O. centrocarpum* percentages that could also relate to local processes, such as enhanced upwelling resulting from changes in the dominant wind pattern (Solignac et al., 2011). The timing of the thermal optimum at our study site overlaps with the one recorded at the other sites, except perhaps for the Bay of Islands, where the lack of age control and low temporal resolution over the last 3500 yr prevent precise chronostratigraphic inference.

The maximum summer SST recorded during the Late Holocene in the SLE is close to 13°C, which is about 2.5°C higher than the local modern average (10.42 ± 2.73°C; Lemay-Tougas, 2014). At the Bay of Islands site off west Newfoundland, Levac (2003) reconstructed February and August SSTs up to 5°C and 2°C higher than at present during the warmest interval of the Common Era. In the GSL, the thermal optimum we identified (1590–1230 cal yr BP) corresponds to summer SSTs of 12°C–14°C, comparable to the one recorded in the SLE but within the range of modern values (14.0 ± 2.1°C).

Regardless of the uncertainties in the reconstruction and chronology of each record, the data together point to relatively warm conditions in the SLE and GSL during the early part of the Common Era. Given the location of our study site in the central GSL, away from the coast and upwelling zones where local processes can impact dinoflagellate populations and dinocyst assemblages, we propose that our reconstructions are representative of changes at the scale of the GSL area. Our record shows that the warmest phase of the Common Era likely occurred from 1590 to 1230 cal yr BP. It also suggests another warm event around 750 cal yr BP (1200 CE), which might correspond to the end of the Medieval Warm Period (e.g., Mann et al., 2009) at regional scale.

The cooling trend of the last millennium and the 170–40 cal yr BP (1780–1910 CE) cold interval

The cooling trend spanning from about 1230 to 40 cal yr BP in our record is a continuum from the upper zone 1 through zones 2 and 3 defined from PCA, which is characterized by increasing percentages of *Islandinium* relative to decreasing percentages of *Brigantedinium* spp. and *B. tepikiense* in the dinocyst assemblages.

The reconstructions illustrate a cooling trend marked by a decrease of ~4°C in surface waters in summer and by increased sea-ice cover from 2 months/yr to 4 months/yr. Similar Late Holocene cooling was reconstructed based on dinocyst assemblages of nearby marine sites (Levac, 2003; Solignac et al., 2011; Lemay-Tougas, 2014). However, unlike the continuous long-term cooling we recorded in the GSL, the data from the SLE rather suggested a cooling event of ~2°C between 1200 and 500 cal yr BP (Lemay-Tougas, 2014). In the Bay of Islands, the Late Holocene cooling has an amplitude of about 3°C (Levac, 2003). In Placentia Bay and Bonavista Bay off southeast and northeast Newfoundland, a shift to fresher/colder conditions is inferred from increasing percentages of *I. minutum* and *Brigantedinium*

https://doi.org/10.1017/qua.2021.56 Published online by Cambridge University Press

spp. (Solignac et al., 2011). The interpretation is qualitative, but the trend is comparable to the one from our record, especially for SST and sea-ice cover (see Fig. 10).

In our record from the central GSL, the latest cooling event is dated 170–40 cal yr BP. It is marked by the coldest conditions of the record, with summer SSTs about 5.5°C lower than the modern average that probably correspond to the regional signature of the LIA (e.g., Lamb, 1995; Mann et al., 2009). It is accompanied by a slight increase of summer SSS (~0.5 psu). While variations of SSS are generally opposite to those of SST in our record, the SLE data from Lemay-Tougas (2014) show parallel variations of SSS and SST with a decrease of ~1.5 psu during the Late Holocene. Such regional differences suggest complex processes in the SLE and the GSL region, which could be further addressed from additional high-resolution records after synchronization and standardization of the time series.

The last 100 yr warming

The upper part of the sequence encompassing the last century corresponds to zone 4 of the dinocyst assemblages. In this zone, *P. dalei* and *S. elongatus* increased, whereas *Islandinium*, *N. labyrinthus*, and *B. tepikiense* decreased. The MAT reconstructions show a warming of about 3°C with decreasing surface salinity and sea-ice cover since about 1910 CE. A recent warming at regional scale was documented from benthic foraminifera that are tracers of the bottom waters (Genovesi et al., 2011; Thibodeau et al., 2013). Our record documents change in surface waters, likely associated with atmospheric conditions. The assemblages, PCA scores, and reconstructions indicate that the last 100 yr experienced unprecedented conditions at the scale of the last two millennia: the PC1 scores indicate unique assemblages of dinocysts, and the reconstructions show a reversal of the long-term cooling trend with summer SSTs rising from the coldest levels of the record toward the lower bound of modern averages; the highest summer primary productivity at 2645 mgC/m^2/day is also recorded during this period (see Figs. 9 and 10). This might partly correspond to the recovery from the LIA but may also be associated with the ongoing anthropogenic climate change.

Insights into climate and ocean changes: regional versus global events

The warm sea-surface conditions recorded between 1590 and 1230 cal yr BP based on dinocyst assemblages correspond to low summer SSS, which suggests high freshwater inputs from the St. Lawrence watershed, and thus high regional precipitation. Sauvé (2016) reconstructed up to 200 mm higher mean annual precipitation than the present at Anticosti Island between ~2500 and ~1500 cal yr BP based on pollen assemblages in peatlands. This is consistent with our data despite the difference in timing that could be due to the accuracy of the chronology in the different records. In eastern Newfoundland, the reconstruction of bog surface wetness showed a major "wet phase" between 1700 and 1200 cal yr BP (Hughes et al., 2006). Hence, wet conditions at the scale of the GSL area during a large part of the first millennium of the Common Era is inferred. The subsequent cooling from 1230 to 40 cal yr BP in our reconstruction is accompanied with a slight increase of SSS, thus suggesting a decrease of regional summer precipitation, especially during cool phases.

A Late Holocene cooling is reported from many palynological studies across eastern Canada (e.g., Marcoux and Richard, 1995; McCarthy et al., 1995; Lavoie and Filion, 2001; Muller et al., 2003; Asnong and Richard, 2005). Signs of cooling characterize the paleovegetation records of the Middle to Late Holocene, and quantitative reconstructions suggest that the amplitude of the cooling trend was larger in summer than in winter (Fréchette et al., 2021). The regional sea-surface cooling trend of about 4°C in summer during the last two millennia was probably part of the long-term climate changes initiated during the Middle Holocene as the result of decreasing summer insolation in the Northern Hemisphere (e.g., Marcott et al., 2013; Kaufman et al., 2020; Fig. 10). The regional cooling trend is characterized by much larger amplitude than the global mean (cf. Marcott et al., 2013; Kaufman et al., 2020), which suggests a higher sensitivity of the GSL surface hydrography and ecosystem to summer insolation. Beyond the long-term cooling recorded from 1230 to 40 cal yr BP that probably relates to decrease in insolation, secular variations in reconstructed SSTs deserve some attention. At our study site, maximum summer SSTs are recorded around 1550 and 1300 cal yr BP (400 and 650 CE), and minimum SST is recorded at ~140 cal yr BP (~1810 CE). Although we cannot discard the possibility that such extremes correspond to noise, high and low SST values probably represent high frequency variations in hydrographical conditions, given the quality of dinocyst data (high counts, high concentrations, short statistical distance of the analogs, etc.). The pacing is comparable to the solar cycles such as the de Vries cycle. The data of Steinhilber et al. (2012), derived from combined records of ^{10}Be in Greenland and Antarctica ice cores and ^{14}C in tree rings (Fig. 10), illustrate major negative excursions of total solar irradiance, some contemporaneous with decreases in SSTs in the GSL at 1290–1180, 700–600, 540–430, and 310–190 cal yr BP. This leads us to suggest linkages of surface-water temperature in the GSL with solar forcing. However, higher temporal resolution in the marine record and other regional data sets would be necessary for a clear demonstration and to identify causal relationships.

The thermal minimum that characterizes our record between 170 and 40 cal yr BP (1780–1910 CE) is consistent with the reconstruction of global temperature by Marcott et al. (2013), who have shown that the Middle–Late Holocene cooling culminated at about 200 cal yr BP during the LIA (e.g., Lamb, 1995; Mann et al., 2009). In the Havre-Saint-Pierre area, north of the GSL, Sauvé (2016) identified particularly cold conditions between 500 and 150 cal yr BP from the peatland pollen record, with mean July air temperatures 1°C below present values. This interval overlaps with our coldest peak, but records smaller amplitude, possibly due to lower sensitivity of pollen data for recording high frequency variation (Webb, 1986). In eastern Newfoundland, based on a composite reconstruction from plant macrofossils, testate amoebae, and the degree of peat humification, Hughes et al. (2006) have identified a shift toward a rise in bog surface wetness at ca. 200 cal yr BP, which suggests wetter and/or cooler conditions. In northeastern Prince Edward Island, higher water-table depths are reconstructed from 550 to 150 cal yr BP using testate amoeba records from Baltic Bog, which also suggest wetter conditions (Peros et al., 2016). According to our data, the LIA was a cold period not necessarily marked by enhanced precipitation, as reconstructed SSS suggests lower freshwater discharge to the GSL. Hence, the wetter conditions inferred from terrestrial records are probably related to reduced evapotranspiration rather than increased precipitation.

A recent warming, starting about one century ago in our record, is also widely documented in regional and global

https://doi.org/10.1017/qua.2021.56 Published online by Cambridge University Press

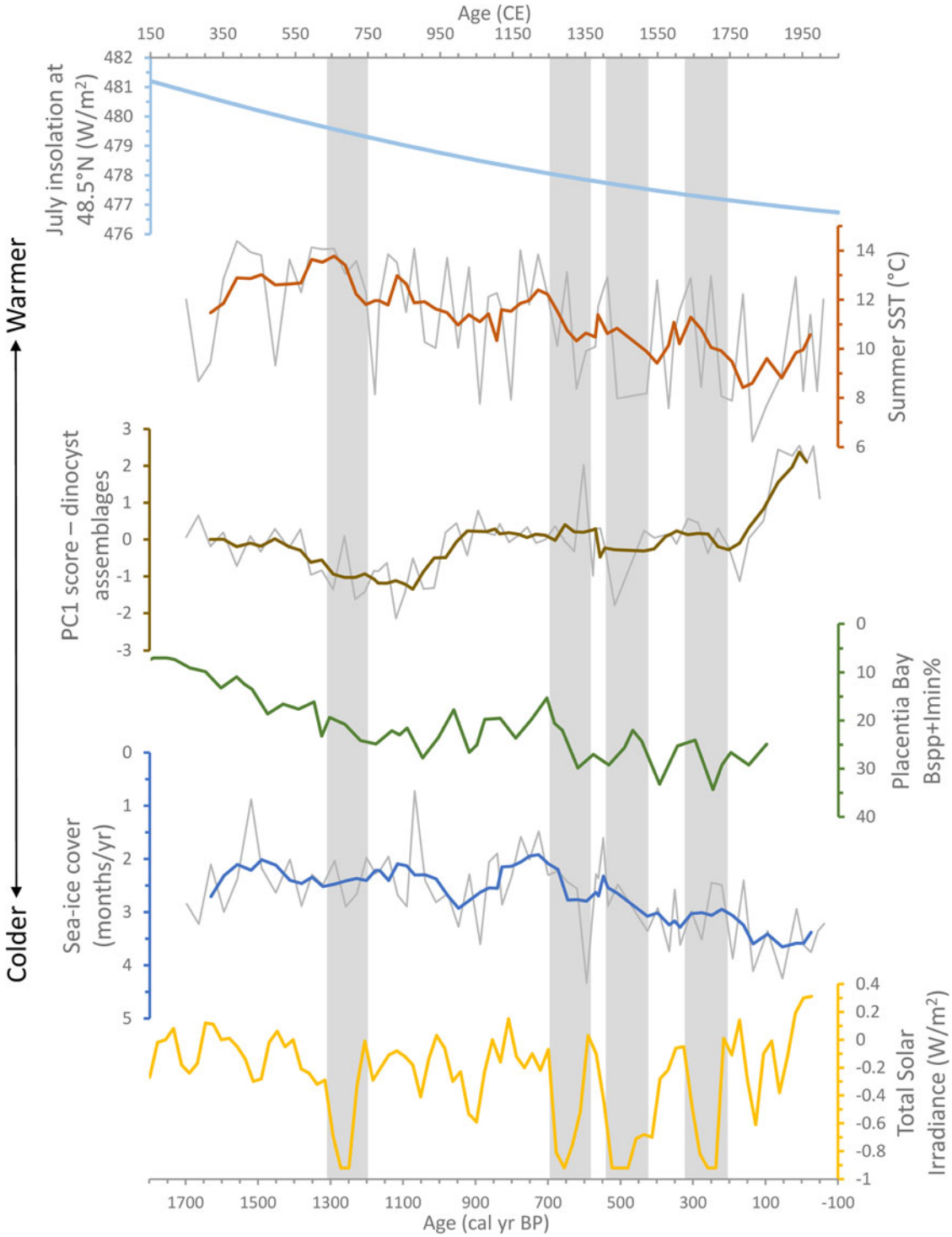

Figure 10. July insolation at the latitude of the core site (48.5°N; light blue curve) from Laskar et al. (2004), SST and sea-ice cover record in core MSM46-03 (red and blue curves), principal component analysis (PCA) axis 1 sample scores of dinocyst assemblages in core MSM46-03 (brown curve), the sum of *Brigantedinium* spp. and *I. minutum* percentages from Placentia Bay (Solignac et al., 2011; green curve), and total solar irradiance anomalies (yellow curve) given as difference to the value of the solar cycle minimum of the year 1986 CE from Steinhilber et al. (2012), https://www.ncdc.noaa.gov/paleo-search/study/12894, accessed September 3, 2020. Gray bands highlight the main negative excursions of solar irradiance. Records from MSM46-03 (this study) were smoothed with a five-point running mean. Note that the axes for sea-ice cover and Bspp+Imin% are reversed to facilitate comparison with other records.

temperature reconstructions (e.g., Thibodeau et al., 2010; Genovesi et al., 2011; Marcott et al., 2013; Kaufman et al., 2020). In contrast to cold and warm intervals of the Late Holocene in eastern Canada that often exhibit poor spatiotemporal coherence, the recent warming shows nearly global coherence over the past 150 yr, which strongly suggests a large-scale forcing

https://doi.org/10.1017/qua.2021.56 Published online by Cambridge University Press

and an anthropic origin for this recent trend (Neukom et al., 2019). In general, there is little evidence for preindustrial globally coherent cold and warm epochs over the Common Era (PAGES 2k Consortium, 2013), suggesting that preindustrial forcings were insufficient or too regional to produce globally synchronous climate changes. Therefore, the study of mechanisms acting at regional scale is also of primary importance, as they seem to have had a large impact on the climate changes of the past two millennia.

CONCLUSION

Our study demonstrates that large variations of sea-surface conditions characterize the GSL area over the past two millennia. Our results showed a distinct thermal optimum of the Common Era, with SSTs comparable to the modern average and low salinities suggesting high precipitation at the scale of the watershed from 1590 to 1230 cal yr BP (360–720 CE). This optimum was followed by a progressive cooling of ~4°C in surface water, with high salinity likely related to low regional precipitation. This cooling culminated between 170 and 40 cal yr BP (1780–1910 CE) and could be associated with the regional signature of the LIA. The 4°C cooling is exceptional in terms of amplitude compared with global temperature reconstructions covering the last 2000 yr (cf. Marcott et al., 2013; Kaufman et al., 2020). This may imply an extremely high sensibility of the GSL surface waters to climate changes, pointing to possibly devastating effects that the ongoing global warming might have on the GSL ecosystem in the future. To confirm this finding, it would be relevant to extend the study to a longer time interval, including the Holocene Climate Optimum, between about 8000 and 6000 cal yr BP, when the climate was globally warmer than the present, conditions associated with high summer insolation (e.g., Marcott et al., 2013; Kaufman et al., 2020).

Comparison with other paleoclimate records and terrestrial palynostratigraphy highlighted the influence of insolation on regional hydrography over the last 2000 yr. It also suggested some changes in regional wind regime in relation to variations of atmospheric circulation patterns over eastern Canada. In hydroclimatic reconstructions derived from peat-based proxy records, it is sometimes difficult to disentangle the signal of high precipitation from low temperature that causes low evapotranspiration, as both lead to high effective moisture. The highly stratified waters of the GSL are largely controlled by continental runoff (Saucier et al., 2003; Galbraith et al., 2012) and thus reflect the difference between precipitation and evaporation at the scale of the watershed. Therefore, the SSS provides an independent indication of hydroclimatic conditions. Our study demonstrated that SSS reconstructed from dinocyst data can provide useful complementary information for the interpretation of regional climate.

Our results and other paleoclimatic records from the GSL area encompassing the last 2000 yr do not show unequivocal signals for the succession of cold and warm phases, such as the Roman Warm Period and the Dark Ages Cold Period, but rather suggest a continuum from warm to cold conditions until the recent warming, with short-lived oscillations that might relate to solar irradiance excursions. Additional high-resolution records from other sites of the GSL may help to better document the regional response of climate changes and their underlying mechanisms.

Supplementary Material. The supplementary material for this article can be found at https://doi.org/10.1017/qua.2021.56.

Acknowledgments. We thank the scientific party of the R/V *Maria S. Merian* for offering the samples from core MSM46-03. This study was supported by the Fonds de Recherche du Québec–Nature et technologies (FRQNT) and the Natural Sciences and Engineering Research Council (NSERC) of Canada. We thank Matthew Peros for constructive comments on an earlier version of the article and Estelle Allan for help in the palynological laboratory. We are grateful to the editor Thomas Lowell and the reviewers Francine McCarthy and Jennifer Galloway for their thoughtful comments and suggestions.

REFERENCES

Agriculture and Agri-Food Canada, 2013. National Ecological Framework for Canada. 2013-05-21 ed. Agriculture and Agri-Food Canada, Government of Canada (accessed April 7, 2020). https://open.canada.ca/data/en/dataset/3ef8e8a9-8d05-4fea-a8bf-7f5023d2b6e1.

Anderson, T.W., 1985. Late-Quaternary pollen records from eastern Ontario, Quebec, and Atlantic Canada. In: Bryant, V.M. and Holloway, R.G. (Ed.), *Pollen Records of Late-Quaternary North American Sediments*. American Association of Stratigraphic Palynologists Foundation, Dallas, Texas, pp. 281–326.

Asnong, H., Richard, P.J.H., 2003. Postglacial vegetation and climate of the central and eastern Gaspésie, Québec. *Géographie physique et Quaternaire* **57**, 37–63.

Balestra, B., Bertini, A., de Vernal, A., Monechi, S., Reale, V., 2013. Late Quaternary sea surface conditions in the Laurentian Fan: evidence from coccolith and dinocyst assemblages. *Palaeogeography, Palaeoclimatology, Palaeoecology* **387**, 200–210.

Behrenfeld, M.J., Falkowski, P.G., 1997. Photosynthetic rates derived from satellite-based chlorophyll concentration. *Limnology and Oceanography* **42**, 1–20.

Blaauw, M., Christen, J., 2011. Flexible paleoclimate age-depth models using an autoregressive gamma process. *Bayesian Analysis* **6**, pp. 457–474.

Bryson, R.A., 1966. Air masses, streamlines and the boreal forest. *Geographical Bulletin* **8**, 228–266.

Bryson, R.A., Hare, F.K., 1974. Climates of North America. In: Bryson, R.A., Hare, F.K. (Eds.), *Climates of North America: World Survey of Climatology*, Vol. 11. Amsterdam: Elsevier. pp. 1–47.

Carcaillet, C., Richard, P., 2000. Holocene changes in seasonal precipitation highlighted by fire incidence in eastern Canada. *Climate Dynamics* **16**, 549–559.

Cauchon-Voyer, G., Henry, M., Desrosiers, G., Lajeunesse, P., Locat, J., Rochon, A., St-Onge, G., 2005. Rapport de mission COR0503, Estuaire et Golfe du Saint-Laurent, 3 au 19 juin 2005. Cruise report. Available at: https://www.geotop.ca/sites/default/files/fichiers/Rapport_Coriolis_2005_0.pdf

Commission for Environmental Cooperation, 1997. Ecological Regions of North America: Toward a Common Perspective. Revised 2006. 1:12,500,000. Commission for Environmental Cooperation, Montreal, Quebec, Canada, 71 pp.

Desprat, S., Sánchez Goñi, M.a.F., Loutre, M.-F., 2003. Revealing climatic variability of the last three millennia in northwestern Iberia using pollen influx data. *Earth and Planetary Science Letters* **213**, 63–78.

de Vernal, A., Giroux, L., 1991. Distribution of organic walled microfossils in recent sediments from the Estuary and Gulf of St. Lawrence: some aspects of the organic matter fluxes. *Canadian Journal of Fisheries and Aquatic Sciences* **113**, e199.

de Vernal, A., Guiot, J., Turon, J.-L., 1993. Late and postglacial paleoenvironments of the Gulf of St. Lawrence: marine and terrestrial palynological evidence. *Géographie physique et Quaternaire* **47**, 167–180.

de Vernal, A., Henry, M., Bilodeau, G., 1999. Techniques de préparation et d'analyse en micropaléontologie. *Les cahiers du GEOTOP* **3**, 16–27.

de Vernal, A., Henry, M., Matthiessen, J., Mudie, P.J., Rochon, A., Boessenkool, K.P., Eynaud, F., Grøsfjeld, K., Guiot, J., Hamel, D., 2001. Dinoflagellate cyst assemblages as tracers of sea-surface conditions in the northern North Atlantic, Arctic and sub-Arctic seas: the new "n = 677" database and its application for quantitative palaeoceanographic reconstruction. *Journal of Quaternary Science: Published for the Quaternary Research Association* **16**, 681–698.

de Vernal, A., Hillaire-Marcel, C., Rochon, A., Fréchette, B., Henry, M., Solignac, S., Bonnet, S., 2013a. Dinocyst-based reconstructions of sea ice cover concentration during the Holocene in the Arctic Ocean, the northern North Atlantic Ocean and its adjacent seas. *Quaternary Science Reviews* **79**, 111–121.

de Vernal, A., Marret, F., 2007. Organic-walled dinoflagellate cysts: tracers of sea-surface conditions. In: Hillaire-Marcel, C., De Vernal, A. (Eds.), *Developments in Marine Geology*. Amsterdam: Elsevier, pp. 371–408.

de Vernal, A., Radi, T., Zaragosi, S., Van Nieuwenhove, N., Rochon, A., Allan, E., De Schepper, S., *et al.*, 2020. Distribution of common modern dinoflagellate cyst taxa in surface sediments of the Northern Hemisphere in relation to environmental parameters: the new n=1968 database. *Marine Micropaleontology*, **159**, 101796.

de Vernal, A., Rochon, A., Fréchette, B., Henry, M., Radi, T., Solignac, S., 2013b. Reconstructing past sea ice cover of the Northern Hemisphere from dinocyst assemblages: status of the approach. *Quaternary Science Reviews* **79**, 122–134.

Dhahri, N., 2010. Natural Variability of Pelagic and Benthic Conditions in the Gulf of St. Lawrence during the Late Holocene. MSc thesis, Université du Québec à Montréal, Canada.

Faegri, K., Iversen, J., 1964. *Textbook of Pollen Analysis*. 2nd ed. New York: Hafner Pub. Co.

Fréchette, B., Richard, P.J.H., Lavoie, M., Grondin, P., Larouche, A.C., 2021. Histoire postglaciaire de la végétation et du climat des pessières et des sapinières de l'est du Québec et du Labrador méridional. Gouvernement du Québec, ministère des Forêts, de la Faune et des Parcs, Direction de la recherche forestière. *Mémoire de recherche forestière* **186**, 170 pp.

Galbraith, P.S., 2006. Winter water masses in the Gulf of St. Lawrence. *Journal of Geophysical Research: Oceans* **111**, C06022. doi:10.1029/2005JC003159.

Galbraith, P.S., Chassé, J., Caverhill, C., Nicot, P., Gilbert, D., Lefaivre, D., Lafleur, C., 2019. *Physical Oceanographic Conditions in the Gulf of St. Lawrence during 2018*. Research Document 2019/046. Department of Fisheries and Oceans, Canadian Science Advisory Secretariat, Ottawa, Ontario.

Galbraith, P.S., Larouche, P., Chassé, J., Petrie, B., 2012. Sea-surface temperature in relation to air temperature in the Gulf of St. Lawrence: interdecadal variability and long term trends. *Deep-Sea Research Part II: Topical Studies in Oceanography* 77–80, 10–20.

Genovesi, L., de Vernal, A., Thibodeau, B., Hillaire-Marcel, C., Mucci, A., Gilbert, D., 2011. Recent changes in bottom water oxygenation and temperature in the Gulf of St. Lawrence: Micropaleontological and geochemical evidence. *Limnology and Oceanography* **56**, 1319–1329.

Gilbert, D., Sundby, B., Gobeil, C., Mucci, A., Tremblay, G.H., 2005. A seventy-two-year record of diminishing deep-water oxygen in the St. Lawrence estuary: the northwest Atlantic connection. *Limnology and Oceanography* **50**, 1654–1666.

Gilliam, F.S., Goodale, C.L., Pardo, L.H., Geiser, L.H., Lilleskov, E.A., 2011. Eastern temperate forests. In: Pardo, L.H., Robin Abbott, M.J., Driscoll, C.T.(Eds.), *Assessment of Nitrogen Deposition Effects and Empirical Critical Loads of Nitrogen for Ecoregions of the United States*. Gen. Tech. Rep. NRS-80. Newtown Square, PA: U.S. Department of Agriculture, Forest Service, Northern Research Station, pp. 99–116.

Guiot, J., de Vernal, A., 2007. Transfer functions: methods for quantitative paleoceanography based on microfossils. In: Hillaire-Marcel, C., De Vernal, A. (Eds.), *Developments in Marine Geology*. Amsterdam: Elsevier, pp. 523–563.

Helama, S., Jones, P.D., Briffa, K.R., 2017. Dark Ages Cold Period: a literature review and directions for future research. *The Holocene* **27**, 1600–1606.

Hughes, P.D.M., Blundell, A., Charman, D.J., Bartlett, S., Daniell, J.R.G., Wojatschke, A., Chambers, F.M., 2006. An 8500 cal. year multi-proxy climate record from a bog in eastern Newfoundland: contributions of meltwater discharge and solar forcing. *Quaternary Science Reviews* **25**, 1208–1227.

Jessen, C.A., Solignac, S., Nørgaard-Pedersen, N., Mikkelsen, N., Kuijpers, A., Seidenkrantz, M.-S., 2011. Exotic pollen as an indicator of variable atmospheric circulation over the Labrador Sea region during the mid to late Holocene. *Journal of Quaternary Science* **26**, 286–296.

Kaufman, D., McKay, N., Routson, C., Erb, M., Dätwyler, C., Sommer, P.S., Heiri, O., Davis, B., 2020. Holocene global mean surface temperature, a multi-method reconstruction approach. *Scientific Data* **7**, 201.

Koutitonsky, V., Bugden, C., 1991. The Physical Oceanography of the Gulf of St. Lawrence: A Review with Emphasis on the Synoptic Variability of the Motion. In: Therriault, J.-C. (Ed.), *The Gulf of St. Lawrence: Small Ocean or Big Estuary?* Canadian Special Publication of Fisheries and Aquatic Sciences 113. Fisheries and Oceans Canada, Ottawa, Ontario, pp. 57–90.

Lamb, H.H., 1995. *Climate, History and the Modern World*. 2nd ed. New York: Routledge.

Laskar, J., Robutel, P., Joutel, F., Gastineau, M., Correia, A.C.M., Levrard, B., 2004. A long-term numerical solution for the insolation quantities of the Earth. *Astronomy & Astrophysics* **428**, 261–285.

Lavoie, M., Filion, L., 2001. Holocene vegetation dynamics of Anticosti Island, Québec, and consequences of remoteness on ecological succession. *Quaternary Research* **56**, 112–127.

Lemay-Tougas, M., 2014. Changements climatiques le long de la Côte Nord de l'Estuaire et du Golfe du Saint-Laurent durant l'Holocène: relation entre les conditions hydrographiques et le développement des tourbières ombrotrophes côtières. Master's thesis, Université du Québec à Montréal, Canada.

Levac, E., 2001. High resolution Holocene palynological record from the Scotian Shelf. *Marine Micropaleontology* **43**, 179–197.

Levac, E., 2003. Palynological records from bay of islands, Newfoundland: direct correlation of Holocene paleoceanographic and climatic changes. *Palynology* **27**, 135–154.

Macpherson, J.B., 1982. Postglacial vegetational history of the eastern Avalon Peninsula, Newfoundland, and Holocene climatic change along the eastern Canadian seaboard. *Géographie physique et Quaternaire* **36**, 175–196.

Magnan, G., Garneau, M., 2014. Evaluating long-term regional climate variability in the maritime region of the St. Lawrence North Shore (eastern Canada) using a multi-site comparison of peat-based paleohydrological records. *Journal of Quaternary Science* **29**, 209–220.

Mäkelä, E.M., 1996. Size distinctions between *Betula* pollen types—a review. *Grana* **35**, 248–256.

Mann, M.E., Zhang, Z., Rutherford, S., Bradley, R.S., Hughes, M.K., Shindell, D., Ammann, C., Faluvegi, G., Ni, F., 2009. Global signatures and dynamical origins of the Little Ice Age and Medieval Climate Anomaly. *Science* **326**, 1256–1260.

Marcott, S.A., Shakun, J.D., Clark, P.U., Mix, A.C., 2013. A reconstruction of regional and global temperature for the past 11,300 years. *Science* **339**, 1198–1201.

Marcoux, N., Richard, P.J.H., 1995. Végétation et fluctuations climatiques postglaciaires sur la côte septentrionale gaspésienne, Québec. *Canadian Journal of Earth Sciences* **32**, 79–96.

McAndrews, J.H., Berti, A.A., Norris, G., 1973. *Key to the Quaternary pollen and spores of the Great Lakes region*. Toronto: Royal Ontario Museum, pp. 1–59.

McCarthy, F.M.G., Collins, E.S., McAndrews, J.H., Kerr, H.A., Scott, D.B., Medioli, F.S., 1995. A comparison of postglacial arcellacean ("thecamoebian") and pollen succession in Atlantic Canada, illustrating the potential of arcellaceans for paleoclimatic reconstruction. *Journal of Paleontology* **69**, 980–993.

McNeely, R., Dyke, A.S., Southon, J.R., 2006. *Canadian Marine Reservoir Ages, Preliminary Data Assessment*. Geological Survey Canada. Open File 5049, 3 pp.

Mertens, K., Verhoeven, K., Verleye, T., Louwye, S., Amorim, A., Ribeiro, S., Deaf, A., Harding, I., De Schepper, S., Gonzalez, C., 2009. Determining the absolute abundance of dinoflagellate cysts in recent marine sediments: the *Lycopodium* marker-grain method put to the test. *Review of Palaeobotany and Palynology* **157**, 238–252.

Mudie, P.J., 1982. Pollen distribution in recent marine sediments, eastern Canada. *Canadian Journal of Earth Sciences* **19**, 729–747.

Muller, S.D., Richard, P.J., Guiot, J., de Beaulieu, J.-L., Fortin, D., 2003. Postglacial climate in the St. Lawrence lowlands, southern Québec: pollen and lake-level evidence. *Palaeogeography, Palaeoclimatology, Palaeoecology* **193**, 51–72.

Neukom, R., Steiger, N., Gómez-Navarro, J.J., Wang, J., Werner, J.P., 2019. No evidence for globally coherent warm and cold periods over the preindustrial Common Era. *Nature* **571**, 550–554.

https://doi.org/10.1017/qua.2021.56 Published online by Cambridge University Press

O'Brien, S.R., Mayewski, P.A., Meeker, L.D., Meese, D.A., Twickler, M.S., Whitlow, S.I., 1995. Complexity of Holocene climate as reconstructed from a Greenland ice core. *Science* **270**, 1962–1964.

PAGES 2k Consortium, 2013. Continental-scale temperature variability during the past two millennia. *Nature Geoscience* **6**, 339–346.

Peros, M., Chan, K., Magnan, G., Ponsford, L., Carroll, J., McCloskey, T., 2016. A 9600-year record of water table depth, vegetation and fire inferred from a raised peat bog, Prince Edward Island, Canadian Maritimes. *Journal of Quaternary Science* **31**, 512–525.

Pollehne, F., 2015. Short Cruise Report *Maria S. Merian* MSM 46 (accessed July 19, 2021). https://www.ldf.uni-hamburg.de/en/merian/wochenberichte/wochenberichte-merian/msm44-msm46/msm46-scr.pdf.

Pratte, S., Garneau, M., De Vleeschouwer, F., 2017. Late-Holocene atmospheric dust deposition in eastern Canada (St. Lawrence North Shore). *The Holocene* **27**, 12–25.

Radi, T., Bonnet, S., Cormier, M.-A., de Vernal, A., Durantou, L., Faubert, É., Head, M.J., *et al.*, 2013. Operational taxonomy and (paleo-)autecology of round, brown, spiny dinoflagellate cysts from the Quaternary of high northern latitudes. *Marine Micropaleontology* **98**, 41–57.

Ramsden, P.G., 1978. Two views on late prehistoric Iroquois trade and settlement: I: An hypothesis concerning the effects of early European trade among some Ontario Iroquois. *Canadian Journal of Archaeology/Journal Canadien d'Archéologie* **2**, 101–106.

R Development Core Team, 2013. *R: A Language and Environment for Statistical Computing*. Vienna, Austria: R Foundation for Statistical Computing.

Reimer, P.J., Bard, E., Bayliss, A., Beck, J.W., Blackwell, P.G., Ramsey, C.B., Buck, C.E., Cheng, H., Edwards, R.L., Friedrich, M., 2013. IntCal13 and Marine13 radiocarbon age calibration curves 0–50,000 years cal BP. *Radiocarbon* **55**, 1869–1887.

Reimer, P.J., Reimer, R.W., 2001. A marine reservoir correction database and on-line interface. *Radiocarbon* **43**, 461–463.

Richard, P., 1970. Atlas pollinique des arbres et de quelques arbustes indigènes du Québec. *Le Naturaliste Canadien* **97**, 1–34, 97–161, 241–306.

Rochon, A., de Vernal, A., 1994. Palynomorph distribution in Recent sediments from the Labrador Sea. *Canadian Journal of Earth Sciences* **31**, 115–127.

Rochon, A., de Vernal, A., Turon, J.-L., Matthiessen, J., Head, M.J., 1999. Distribution of recent dinoflagellate cysts in surface sediments from the North Atlantic and adjacent seas in relation to sea-surface parameters. *American Association of Stratigraphic Palynologists Contribution Series* **35**, 1–146.

Saucier, F.J., Roy, F., Gilbert, D., 2003. Modeling the formation and circulation processes of water masses and sea ice in the Gulf of St. Lawrence, Canada. *Journal of Geophysical Research* **108** (C8), 3269.

Sauvé, A., 2016. Reconstitution Holocène de la végétation et du climat pour les régions de Baie-Comeau et d'Havre-Saint-Pierre, Québec. Master's thesis, Université du Québec à Montréal, Canada.

Seidov, D., Baranova, O.K., Johnson, D.R., Boyer, T.P., Mishonov, A.V., Parsons, A.R., 2016. Northwest Atlantic Regional Climatology. Regional Climatology Team, *NOAA/NCEI*. www.nodc.noaa.gov/OC5/regional_climate/nwa-climate, dataset: doi:10.7289/V5RF5S2Q (accessed August 17, 2020).

Sicre, M.A., Weckström, K., Seidenkrantz, M.S., Kuijpers, A., Benetti, M., Masse, G., Ezat, U., *et al.*, 2014. Labrador current variability over the last 2000 years. *Earth and Planetary Science Letters* **400**, 26–32.

Solignac, S., Seidenkrantz, M.-S., Jessen, C., Kuijpers, A., Gunvald, A.K., Olsen, J., 2011. Late-Holocene sea-surface conditions offshore Newfoundland based on dinoflagellate cysts. *The Holocene* **21**, 539–552.

Steinhilber, F., Abreu, J.A., Beer, J., Brunner, I., Christl, M., Fischer, H., Heikkila, U., *et al.*, 2012. 9,400 years of cosmic radiation and solar activity from ice cores and tree rings. *Proceedings of the National Academy of Sciences USA* **109**, 5967–5971.

ter Braak, C., Šmilauer, P., 2012. *Canoco Reference Manual and User's Guide: Software of Ordination (Version 5.0)*. Microcomputer Power, Ithaca, NY.

Thibodeau, B., de Vernal, A., Hillaire-Marcel, C., Mucci, A., 2010. Twentieth century warming in deep waters of the Gulf of St. Lawrence: a unique feature of the last millennium. *Geophysical Research Letters* **37**(17).

Thibodeau, B., de Vernal, A., Limoges, A., 2013. Low oxygen events in the Laurentian Channel during the Holocene. *Marine Geology* **346**, 183–191.

Viau, A.E., Gajewski, K., Fines, P., Atkinson, D.E., Sawada, M.C., 2002. Widespread evidence of 1500 yr climate variability in North America during the past 14 000 yr. *Geology* **30**, 455–458.

Webb, T., 1986. Is vegetation in equilibrium with climate? How to interpret late-Quaternary pollen data. *Vegetatio* **67**, 75–91.

Zonneveld, K.A.F., Versteegh, G., Kodrans-Nsiah, M., 2008. Preservation and organic chemistry of Late Cenozoic organic-walled dinoflagellate cysts: a review. *Marine Micropaleontology* **68**, 179–197.

https://doi.org/10.1017/qua.2021.56 Published online by Cambridge University Press